2.4 Linac

2.4.1 Introduction

The main Linac of the Cornell Energy Recovery Linac (ERL) comprises 64 cryomodules each containing 6 superconducting cavities and a superferric quadrupole and steering-corrector package. Section 1.3 explains the need for employment of superconducting cavities. The Linac occupies 700 m of underground tunnel and serves to accelerate the beam from injection energy, 15 MeV, to 5 GeV and decelerate again to approximately the injection energy after passing through the x-ray-producing insertion devices as depicted in Fig. 2.1.2 (ERL Extension of CESR). The superconducting cavity units of the cryomodules and the cryogenic shields are maintained at temperature by a helium cryogenic plant located above the tunnel. Each cavity is individually driven by an RF power source with amplitude and phase controlled by low-level RF circuitry adjacent to the cryomodules. The supporting utilities and cryogenics are described in Chapter 4.

State of the art of superconducting RF

Accelerator facilities utilizing superconducting cavities with elliptical shape are becoming prevalent around the world. As new machines continue to push the limits of low emittance and higher-duty cycle, the large iris and low loss of superconducting cavities enable the realization of beam-performance goals. The cavity-performance parameters of other superconducting RF-based facilities are listed in Tab. 2.4.1. The FLASH facility is the most relevant to the Cornell ERL design as it is the product of many years of SRF cavity and cryomodule development now known as the TESLA Technology Collaboration (TTC), and is the basis for this ERL Linac design. This technology is the precursor of the European XFEL facility [1] and it is also the basis for development of the International Linear Collider (ILC) [2]. The result of the many years of TTC development is a cryomodule configuration known as TTF-III that accomplishes reliable performance of the numerous components, a minimal cryogenic heat load, ease of fabrication, and minimization of cost. A photograph of a TTF-III cryomodule in the FLASH tunnel at DESY is shown in Fig. 2.4.1.

Advances in SRF-cavity performance are occurring continuously, as evidenced by the proposed facilities' parameters, which have been obtained in developmental tests, as mentioned in Tab. 2.4.1. The parameters of the Cornell ERL resulted from an optimization encompassing the full machine as described in §2.4.2 below.

Principles governing the baseline design

The ERL Linac design is based on TTF-III technology with modifications for continuous wave (CW) operation. This builds upon the considerable development work performed for this Linac technology over the past 15 years. TTF-III technology is at the forefront of SRF Linac performance in regard to cavity gradient, quality factor Q, power coupled to the beam, cavity tuning, minimal cryogenic heat load, industrial fabrication, and operational reliability. This technology is characterized by module-vacuum vessels joined end-to-end with large lengths of the Linac sharing a common insulation vacuum. For the baseline design, the ERL Linac will have a north and a south section; the north will have 35 modules and is 344 m long, and the

Table 2.4.1: Accelerator facilities utilizing superconducting RF elliptical cavities.

Facility	Type	Frequency (GHz)	Temperature (K)	Cavity Type	Q at Operational Gradient	Operational Gradient (MV/m)
FLASH	e^- Linac	1.3	1.8	9-cell	1×10^{10}	23
JLAB	e^- Linac	1.497	2.1	5-cell	5×10^9	7.5
Cornell	Test cryomodule	1.3	1.8	7-cell	3×10^{10}	16
SNS	p^+ Linac	0.805		6-cell	5×10^9	8-12
CESR	e^--storage ring	0.5	4.5	1-cell	1×10^9	5-8
KEK-B	e^--storage ring	0.5	4.5	1-cell	2×10^9	4-7
LEP-II	e^+-e^--stor. ring	0.35	4.5	4-cell	3.2×10^9	6
LHC	p^+-p^--stor. ring	0.4	4.5	4-cell	2×10^9	5
Proposed or under construction						
XFEL	e^- Linac	1.3	2.0	9-cell	1×10^{10}	23.6
Cornell ERL	e^- Linac	1.3	1.8	7-cell	2×10^{10}	16
JLAB upgrade	e^- Linac	1.497	2.1	7-cell	6×10^9	17.5
ILC	e^- Linac	1.3	2.0	9-cell	1×10^{10}	31.5

south will have 29 modules and is 285 m long. Placement of an insulation-vacuum break in each of the long Linac sections is under study.

The modifications to the TTF-III technology for CW operation and energy recovery have significant operational differences. From a facility point of view, because the resistive power dissipated in the SRF cavities is absorbed by the refrigeration system at 1.8 K, having CW cavity operation makes the refrigeration system a major utility component. This favors relatively low-cavity gradient as cryogenic power per unit length scales as the square of the gradient. Another consideration that favors lower gradient is that field emission and consequent radiation produced within a given cavity scale exponentially with cavity gradient. This not only adds to the cryogenic load but will also produce a significant radiation level in CW operation. A lower cavity gradient will lessen field emission, and thus shielding requirements.

Achieving as high a cavity Q as possible at a given temperature has a direct benefit of reducing the size of cryoplant. There are three components needing control for highest Q: the BCS component with exponential temperature dependence; the temperature-independent residual resistance, which depends on the surface processing; and the trapped magnetic flux component, which depends on the effectiveness of the magnetic shielding. The latter requires the magnetic shielding in the cryomodule to reduce the background magnetic fields at the cavities to $< 2\,\mathrm{mG}$ to ensure that residual RF losses due to flux pinning are negligible. This will be accomplished by using a demagnetized carbon-steel-vacuum vessel, a mu-metal lining of the vacuum vessel at 293 K, and a shield around each cavity using material formulated for optimal magnetic performance at 1.8 K. With cavity Q dominated by BCS resistance, selection of the cavity temperature then becomes an optimization of refrigeration power and scaling of the BCS resistance with temperature, which favors a cavity temperature of 1.8 K [3].

Reliability and uninterrupted run time of the ERL light source is a performance goal for the

Figure 2.4.1: A photograph of a TTF-III cryomodule in the FLASH tunnel at DESY.

machine. With the Linac total of 384 SRF cavities, the trip rate per cavity needs to be below once per several years to accomplish a machine trip rate of less than once per day. A modest cavity gradient will play a major role in making this feasible, since it has been demonstrated at all of the facilities listed in Table 2.4.1 that operation of SRF cavities is extremely reliable if the cavity gradient and input RF power are not pushed to the limits. The input RF power to each cavity is low due to the energy recovery, typically 2 kW average and 5 kW peak power, so trips due to RF couplers should occur at a very low rate.

The RF-source architecture is likewise designed for reliable machine operation; there will be a dedicated source for each cavity. With this configuration, the loss of one RF source translates to the loss of only one cavity. Having a dedicated source per cavity also allows the flexibility to tune for the best performance of each cavity, which in conjunction with gradient and RF power overhead, will be utilized to compensate for a tripped cavity to provide uninterrupted machine operation. The challenge to the RF system will be in the form of the high loaded quality factor Q_{ext} of the input couplers. This will place tight constraints on maintaining the RF field phase and amplitude in both absolute terms along the length of the Linac and in local terms due to microphonic perturbations of individual cavities. The RF feedback system will be capable of compensating for microphonic perturbations at the expense of increased average

forward power, as demonstrated in the ERL-injector prototype at Cornell. An important developmental task will be to show that the fast-piezo component of the cavity tuner can be used to mechanically compensate for microphonics, and thus lower the Linac RF-power budget.

The short bunch length of 0.6 mm ($\approx 2\,\mathrm{ps}\cdot c$) and high average beam current of 100 mA CW in both the accelerating and decelerating beams in the ERL demands heavy damping of the higher order modes (HOMs) in the cavities. The loaded Q's of such modes and their shunt impedance place direct limits on the beam-breakup (BBU) limited-beam current. The average HOM power is expected to be 200 W per cavity, assuming no resonant excitation of any particular mode. Most of the power will be in the frequency range of 1-10 GHz, but the short bunch length will contain HOM spectral content up to the 100 GHz range. The HOM damping scheme must have strong coupling over this broad bandwidth and be able to dissipate the average power. Beamline-HOM loads have been chosen in the baseline design to accomplish these requirements. The beamline loads will operate at 100K to minimize the cryoplant load, and thus necessitate thermal gradients along the beamline between cavities by way of cooled intercepts. Operation of the ERL-injector prototype at Cornell has given important insight as to the requirements of the RF-absorbing material in the beamline loads, and new robust materials have been developed as a result. The alternate use of waveguide and loop-HOM couplers are the subjects of ongoing investigations [4–6], and while they have the benefit of transporting the HOM power to external-room temperature loads, it is still to be determined if they will have the requisite bandwidth and power capability, and how the structural complexity will compare to beamline loads. Another consequence of the short bunch length and high HOM frequencies is that the design of the mechanical contour of the beamline must have careful consideration of any features with dimensions of $\sim 0.6\,\mathrm{mm}$ or larger, such as flange gaskets and RF pickups, to avoid excitation of high frequency modes and consequent heating.

Another departure from TTF-III technology necessitated by ERL CW operation is the much higher consumption of 1.8 K superfluid helium per cavity and its return gas load. At the cavity level, the helium vessel must have a large aperture to the superfluid reservoir to allow conduction of the nominal 12 W heat flow per cavity. At the module level, standard TTF-III technology incorporates a single superfluid-helium manifold joined between modules to run the entire length of a Linac section, with a feed from one end of the Linac. For the ERL, this configuration would present too much flow restriction; consequently the baseline concept has a larger helium source manifold, and a JT valve supplying a superfluid reservoir per module. The needed design is being developed. As the ERL developmental projects proceed and the design matures, there will also likely be advances in aspects of TTF technology from the ILC and XFEL programs, including cost reductions and industrialization. Cornell has close communication and collaboration with these projects and will share in such benefits as a long-standing member of the TTC. Cornell is also serving as a major partner in the Daresbury ERL demonstration project, providing the 7-cell SRF cavities and technical consultation [7]. Other collaborations are forming for ERL development work, such as microphonic compensation with the Helmholtz Zentrum Berlin (HZB) and RF-absorber material development for HOM loads with the Ningbo Institute of Material Technology and Engineering (NIMTE) in China, the Spheric and Coorstech Companies and Alfred University in the United States.

In the sections that follow, the details of many of the ERL-Linac cryomodule components
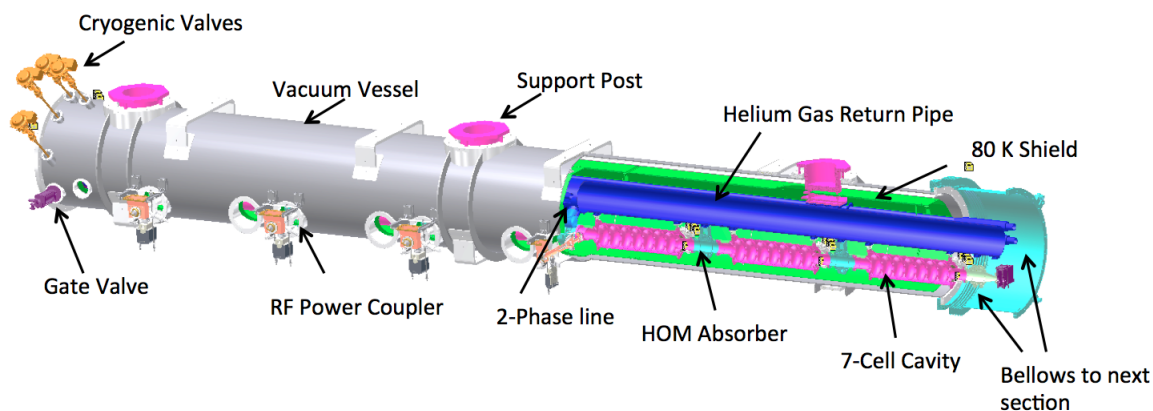
Figure 2.4.2: Cross section of the ERL main Linac cryomodule.

will be described. These features were heavily influenced by experience with the injector-cryomodule prototype (see §2.3.6). A cut-away CAD model of the Linac cryomodule is shown in Fig. 2.4.2, which includes only its main features. The design incorporates six 7-cell SRF cavities, beamline HOM loads, coax-RF couplers, one quadrupole, one set of X-Y steering coils, and gate valves at each end. This cryomodule is 9.82 m long. As a point of reference, Tab. 2.4.2 lists the beamline components of the cryomodule and their lengths.

2.4.2 Cavity

The superconducting cavities in the main Linac of the ERL significantly influence the performance, cost and reliability of the accelerator in several ways. The design of the cavity must be optimized according to the ERL specific requirements.

   The optimization of the main Linac cavity design is driven by the three primary objectives:

- The cavities must be able to support beam currents up to the design value of $2 \times 100\,\mathrm{mA}$, and strong suppression of Higher-Order-Modes (HOM) in the main Linac is therefore essential. In addition, fluctuations in the HOM frequencies from cavity to cavity are desirable to reduce coherent effects and thereby increase the BBU threshold current.

- A large value of R/Q for the fundamental mode (at 1.3 GHz) is highly desirable to minimize the dynamic cryogenic load by the accelerating RF field in the cavities.

- The performance of the cavity design must be robust under small shape imperfections, which are always present due to finite fabrication tolerances.

   Linked to the cavity design are the operating parameters of the cavity. Most of these can be chosen and optimized freely (within certain boundaries). The intrinsic quality factor Q_0 of the cavity is not a free parameter, and it is crucial to assume a realistic value for it, since it determines the size of the cryogenic refrigerator required. The following sections discuss the ERL main Linac cavities and their baseline operating parameters in detail. Subsequent sections present the RF and mechanical design of the main Linac cavities in detail, including the choice

Table 2.4.2: Beamline components and lengths of the Linac cryomodule.

	Component	Length (m)
	Gate Valve	0.0750
	Taper	0.0500
Repeat 6 times	HOM Absorber	0.0600
	110mm Cu beam tube	0.0476
	110mm Nb beam tube	0.2150
	Cavity active length	0.8061
	110mm Nb beam tube	0.2150
	110mm Cu beam tube	0.0476
	HOM Absorber	0.0600
	Taper	0.0500
	BPM	0.0750
	Quadrupole	0.4500
	X-Y Steering Coils	0.1500
	Gate Valve	0.0750
	Intermodule flex	0.4885
	Module Length	9.8213
	Fill Factor	0.49

of cavity flanges, the LHe vessel design, and the inner magnetic shielding of the cavity. The final sections briefly cover the fabrication of the cavities and their surface preparation.

Frequency choice

The choice of frequency f_0 of the accelerating mode of the main Linac cavity is determined by several factors. These include heat-load considerations, HOMs and the resulting beam breakup current, availability of RF-power sources, as well as the maximum bunch repetition and the minimum bunch charge at given beam current.

The cryogenic losses of a cavity can be separated into static and dynamic losses. It is desirable to minimize these losses since they are the main driver of an ERL's operation cost. For a given length of a multi-cell cavity, the surface area scales with $1/f_0$. The static heat load per length therefore, tends to scale also with $1/f_0$ (assuming that wall thicknesses are unchanged). The surface resistance of the superconductor scales as f_0^2 at higher temperatures where the BCS resistance dominates, and becomes approximately frequency independent at lower temperatures where the residual resistance dominates. Accordingly, the intrinsic quality factor $Q_0 = G/R_S$ scales with $1/f_0^2$ at higher temperatures and is independent of frequency at lower temperatures. For the same accelerating gradient and the same active cavity length, the stored energy U in the cavity per length L scales with $1/f_0^2$ (i.e., with the volume of the cavity per length). The dynamic power dissipated in the walls of a cavity is given by

$$\frac{P_{\text{diss}}}{L} = \frac{2\pi f_0 \, U}{Q_0 L} \, . \tag{2.4.1}$$

Accordingly the dissipated power per active cavity length scales linearly with frequency at higher temperatures and with $1/f_0$ at lower temperatures.

State-of-the-art multi-cell cavities show residual surface resistances of 5 to $10\,\mathrm{n\Omega}$. Taking this into account as well as the frequency and temperature dependences of the BCS surface resistance and the efficiency dependence of the refrigerator on operating temperature, one finds that an operating temperature of 1.8 K reduces the AC cooling power at all frequencies between 500 and 1500 MHz. At this temperature, residual resistance dominates over the BCS resistance, favoring the higher frequencies [8, 9]. In addition, the risk of surface contamination and field emission increase with surface areas, also favoring the higher frequencies.

In regard to the BBU threshold, one notes that for large return times, and for ERLs with many cavities, the threshold current does not strongly depend on the return time. It is then true that there is a reciprocal relation between threshold current and the HOM frequency f, assuming that R/Q and Q of a given mode remains unchanged, which is the case if the number of cells per cavity is unchanged. Decreasing the fundamental frequency from 1.3 GHz to 650 MHz would therefore increase the threshold current by a factor of 2. This strategy of increasing the threshold current has several problems. First, as discussed above, it would significantly increase the AC power required to cool the SRF cavities. Second, to obtain the same average current, the bunch charge would have to be larger, which strengthens space-charge forces and therefore increases the emittance of the electron beam thereby decreasing the spectral brightness of x-ray beams, which is the ultimate quality factor of an ERL design.

The Cornell ERL main Linac is based on 1.3 GHz SRF cavities. This frequency minimizes operating costs, supports operation at the design beam current of 100 mA, as shown in the following sections, and allows the ERL main Linac to make use of the extensive technology developed for the International-Linear-Collider and the XFEL, which are also based on 1.3 GHz superconducting RF.

Cavity operating parameters: Q_0, E_{acc}, and Q_{ext}

The three main cavity operating parameters are the intrinsic quality Q_0 factor of the SRF cavity (which also depends on the operating temperature T), the operating accelerating field gradient E_{acc}, and the external quality factor Q_{ext}. All three parameters strongly impact the ERL main Linac design and cost. While the intrinsic quality factor is determined by the cavity preparation, the operating temperature and the magnetic shielding in the cryomodule, the other two parameters can be chosen freely (within limits).

Intrinsic Q_0 and operating temperature

The dynamic power dissipated in the walls of a single cavity by the accelerating RF field during operation is given by

$$P_{\mathrm{cavity}} = \frac{V_{\mathrm{acc}}^2}{2\frac{R}{Q}Q_0}\,, \tag{2.4.2}$$

where V_{acc} is the accelerating cavity voltage, and (R/Q) is the ratio of cavity shunt impedance to cavity intrinsic quality factor, which is a shape dependent factor. The total dynamic cavity
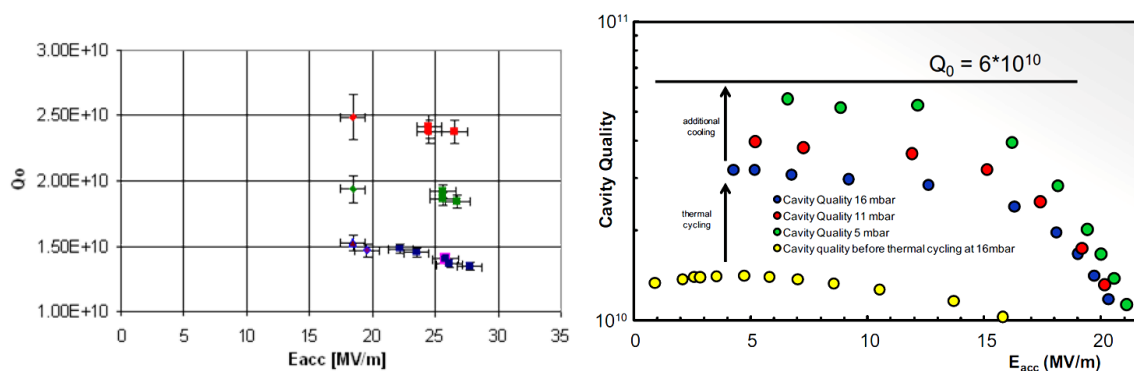
Figure 2.4.3: State-of-the-art performance of fully equipped 9-cell SRF cavities. Left: Average performance of eight 9-cell cavities in a FLASH cryomodule at DESY at different operating temperatures (red: 1.6K, green: 1.8K, blue: 2K). Right: Performance of a 9-cell cavity in a horizontal test cryomodule at different temperatures (16 mbar corresponds to 1.8K) [8, 9].

power in the ERL main Linac is then

$$P_{\text{total}} = \frac{V_{\text{total}}E_{\text{acc}}}{2\frac{R/Q}{L_{\text{cav}}}Q_0}, \tag{2.4.3}$$

where L_{cav} is the active length of the cavity. In case of the ERL, the total accelerating voltage of the main Linac is $V_{\text{total}} = 5\,\text{GV}$, resulting in a significant total power dissipated at the operating temperature of the cavities of the order of several kW. It is obvious that the intrinsic quality factor has dramatic impact on the size of the cryogenic refrigerator and on the capital and operating cost of the ERL. The intrinsic quality factor depends on the so-called geometry factor G of the cavity (determined by its cell shape) and the surface resistance R_{s} of the superconducting material used for the cavity walls: $Q_0 = G/R_{\text{s}}$. As noted above, state-of-the-art multi-cell cavities now exhibit residual resistances of 5 to $10\,\text{n}\Omega$. At 1.8 K this results in Q_0 of 2×10^{10} to 4×10^{10}.

Fully equipped state-of-the-art multi-cell cavities, installed in cryomodules, have achieved quality factors of 2×10^{10} to 3×10^{10} at medium field gradients of about 15 MV/m (see Fig. 2.4.3). It should be noted that the graph on the left side of Fig. 2.4.3 shows the average performance of all eight 9-cell cavities installed in one cryomodule in the FLASH accelerator. Based on these proof-of-principle measurements, an average quality factor of 2×10^{10} at the operating field gradient is assumed for the ERL main Linac at an operating temperature of 1.8 K. This corresponds to the requirement that the residual surface resistance has to be $10\,\text{n}\Omega$ or less.

Very high intrinsic quality factors have also been achieved during the first cryomodule test of the Cornell ERL main linac cavity. The cavity received a bulk buffer-chemical polish (BCP) of $150\,\mu\text{m}$, was heat treated at 800 C for two hours, received a final $10\,\mu\text{m}$ BCP, two eight-hour high pressure rinses, and then was baked under vacuum at 120 C for 48 hours. The cavity was installed in a one-cavity Horizontal Test Cryomodule (HTC) for a first horizontal cryomodule test of the cavity. In order to understand the details on preserving high cavity
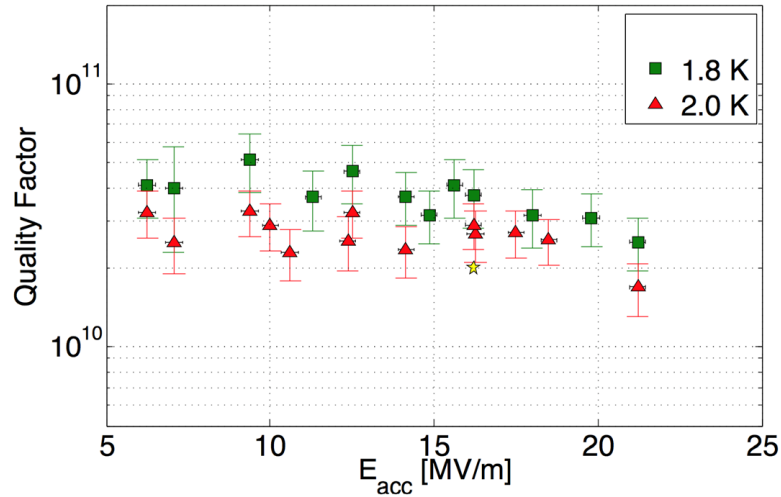
Figure 2.4.4: Intrinsic quality factor vs accelerating field curve at 1.6 K and 1.8 K for the prototype Cornell ERL main linac cavity installed in a test cryomodule. This cavity is fully equipped with power couplers and higher order mode dampers [11].

Q's under different operational configurations, a three step approach was chosen. During the first cryomodule test of the cavity, measurements were done using only a small probe coupler. The performance of the cavity installed in the test module significantly exceeded the 2×10^{10} specification, reaching quality factors at $E_{\mathrm{acc}} = 16.2\,\mathrm{MV/m}$ of $Q_0 = 3 \times 10^{10}$ at 1.8 K and $Q_0 = 4 \times 10^{10}$ at 1.6 K. At lower fields, the quality factor even reached $Q_0 = 6 \times 10^{10}$ at 1.6 K [10]. In a second setup (HTC-2), the final power couplers were mounted and the cavity was re-measured, resulting in only minor changes of the Q-factor. In a third and now final step, the HOM absorbers were mounted reflecting exactly the geometric and EM design of the full linac cavity setup proposed within this report. The performance of the cavity in this full setup is given in Fig. 2.4.4, clearly indicating the performance above specifications. During dismounting of HTC-2 and mounting of HTC-3 the cavity was chemically reprocessed. For details and references to the different treatment and testing steps see [10].

Accelerating gradient

The optimal accelerating field gradient in the cavities of the main Linac is set by considerations of cost of the main Linac (construction and operation cost), the increase in cavity trip rate and electron field emission at higher field gradients. The approach taken is to find the gradient region at which cost is minimized, and then to select a field gradient at the lower end of that region to maximize accelerator availability and to minimize any potential risks from electron field emission. The detailed cost model used for optimization includes the construction costs of the main Linac cryomodules of the RF system including RF power sources, of the cryogenic refrigerator, and of the tunnel length occupied by the main Linac. The total energy gain in the main Linac of a 100 mA beam is fixed at 5 GeV, while the accelerating field gradient in the cavities (and thereby the number of cavities) is varied to yield costs. The main conclusion from

these studies is that the region of minimal cost is quite broad. The model used here shows that the construction costs are the same within 5 % for medium field gradients between 14.5 MV/m and 28 MV/m, with the actual minimum at 18 MV/m. The broad region of minimal cost is a result of the fact that the length of the main Linac and the number of cavities decrease linearly with gradient, but the total dynamic heat load of the cavities in continuous operation and the total RF power required for operating the cavities increase linearly with gradient. Cost studies for other SRF projects have resulted in the same conclusion that medium field gradients in the 15 to 20 MV/m range are optimal for CW Linac [12]. Selecting an accelerating field gradient at the lower end of the 14.5 MV/m to 28 MV/m optimal region is highly advisable for several reasons:

- The size of the 1.8 K cryogenic refrigerator increases linearly with gradient (neglecting static heat loads at 1.8 K, which are small compared to the dynamic cavity load), and so does the AC power and the operating cost of the cryogenic plant. At present, refrigeration plants up to about 5 kW at 1.8 to 2 K are in operation (e.g., CEBAF, LHC).

- The operating cost strongly increases with field gradient, since the total dynamic heat load in the cavities and the total RF power required for operating the cavities increase linearly with gradient.

- The risk of electron field emission increases exponentially with field gradient. Measurements at the FLASH Linac at DESY have shown that detectable field emission in state-of-the-art cavities starts at gradients of $\sim$ 15 to 20 MV/m, and increases by an order of magnitude every 3 to 5 MV/m [13]. Field emission generates captured dark current, reduces the quality factors of the SRF cavities, and generates radiation (x-ray and neutron) in the tunnel. All of these effects are highly undesirable and staying near or below the onset of field emission is therefore advisable.

- Accelerating field gradients in the 15 to 20 MV/m range are nowadays achieved routinely with yields near 100 %. Gradient specifications in this medium field range can significantly simplify the surface treatment of the cavities. Standard chemical etching with BCP (HF, HNO_3 and H_3PO_4, usually in a ratio of 1:1:1 or 1:1:2) is sufficient to yield gradients in this range. Treatment of the cavity surface by the more complex method of electropolishing is only required if it would routinely result in lower residual resistances. This is a topic of ongoing SRF cavity research at numerous laboratories around the globe.

These considerations have led to a baseline specification of the accelerating field gradient in the cavities of the ERL main Linac of 16.2 MV/m, which is at the lower end of the 14.5 MV/m to 28 MV/m optimal cost region. The corresponding cavity dynamic heat load at 1.8 K is $\sim 4\,\mathrm{kW}$.

Cavity external Q_{ext}

In the main Linac of an ERL, the optimal loaded Q_{ext} of the SRF cavities is set by the microphonics level. 'Microphonics' refers to the detuning of an RF cavity by external sources like ground vibrations or LHe bath pressure fluctuations. These vibration sources can couple

Table 2.4.3: Measured microphonic levels measured in SRF Linacs [14].

machine	σ (Hz)	6σ (Hz)	Comments
CEBAF	2.5 (average)	15 (average)	significant fluctuation between cavities
ELBE	1 (average)	6 (average)	
SNS	1 to 6	6 to 36	significant fluctuation between cavities
TJNAF FEL	0.6 to 1.3	3.6 to 7.8	center cavities more quiet
TTF	2 to 7 (pulsed)	12 to 42 (pulsed)	significant fluctuation between cavities

to the cavity via multiple paths. It is useful to distinguish between random noise and defined frequency vibrations. When a vibration source frequency lines up with a mechanical resonance of a cavity, particularly strong microphonics can occur.

Maintaining low cavity microphonic levels is of great importance for an ERL. The main Linac cavities have virtually zero beam loading (the energy transfer from the decelerated beam to the RF-cavity fields compensates the energy transfer from the RF fields to the accelerated beam), and so for efficient cavity operation they should be operated at a very high loaded quality factor Q_{ext}. The optimal Q_{ext} is solely determined by the ratio of the fundamental mode frequency f_0 and the typical detuning Δf

$$Q_{\mathrm{ext,optimal}} = \frac{f_0}{2\Delta f} \, . \tag{2.4.4}$$

The required RF power is directly proportional to the detuning. In designing an ERL, it is therefore extremely important to have a good estimate of the peak cavity detuning when determining the required RF peak power. If one underestimates the peak detuning, and thus the installed RF power is not sufficient, the RF source will run against its maximum output power, and so the cavity is likely to trip every time the cavity detuning exceeds the estimated peak detuning.

Most existing $v_{\mathrm{p}} \approx c$ superconducting RF accelerators have significant beam loading. Because of the resulting relatively high fundamental mode bandwidth (typically between 100 Hz and a few 1 kHz), microphonics is of lesser concern in such machines. Accordingly only limited effort has been made in the past in measuring microphonics, understanding its sources, and improving the mechanical design of the cavities and cryostat to minimize microphonics. Table 2.4.3 summarizes measured rms microphonics levels for different superconducting machines. The peak cavity detuning is estimated as 6σ. In all cases significant fluctuation in microphonics has been found from cavity to cavity, even within the same cryomodule. Table 2.4.3 shows that proofs of principle for low microphonics SRF cryomodules exist, with a peak detuning below 10 Hz appearing feasible if care is taken during the cryomodule design to minimize excitation of cavity vibrations. To be conservative, our parameters assume a peak detuning of 25 Hz.

Assuming 10 Hz as typical peak detuning of the SRF cavities in the ERL main Linac results in a baseline loaded quality factor of 6.5×10^7 and a typical RF-peak power of $\sim 2\,\mathrm{kW}$ per cavity. For some individual cavities and in some rare events, larger cavity detunings should be expected. To prevent cavity trips and beam loss in these cases, 5 kW of RF power will
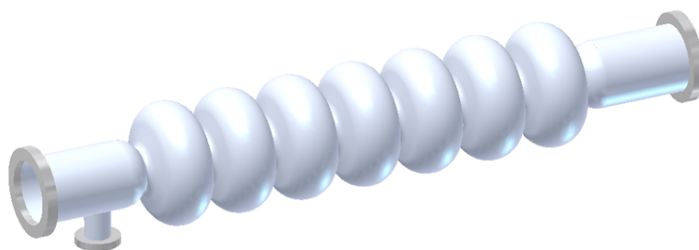
Figure 2.4.5: CAD model of the 7-cell ERL main Linac cavity.

be installed per cavity in the ERL main Linac, allowing maximal detuning during these rare events of up to 25 Hz.

Passive and active means will be used to reduce microphonics in the main Linac cavities below the levels listed in Tab. 2.4.3. As discussed in the following sections in greater detail, the mechanical design of the cavities and of the cryomodule will include microphonics considerations. Besides designing the cryomodule for minimal microphonics, a further reduction in microphonics amplitude could potentially be achieved with active control schemes, making use of a fast frequency tuner. Initial studies have shown promising results [15].

The baseline ERL cavity

This section discusses the RF and mechanical design of the baseline main Linac superconducting RF cavity. The baseline cavity is a standing-wave 7-cell structure of solid niobium with a fundamental mode frequency of 1.3 GHz (see Fig. 2.4.5). Power is coupled into the cavity via one coaxial RF input power coupler located at an end-beam tube. Large diameter beam tubes ensure propagation of all monopole and dipole HOMs to beam tube RF absorbers located between the individual cavities to ensure strong suppression of HOMs and thereby support operation of beam currents up to 100 mA. The cells of the cavity are surrounded by a LHe tank to immerse the cavity into 1.8 K LHe. Each cavity is further equipped with a frequency tuning system (slow tuner driven by a stepping motor and fast tuner driven by piezoelectric crystals), and a field pick-up probe to monitor the cavity-RF fields. Table 2.4.4 summarizes the main parameters of the main Linac cavity. The following subsections give more details on the cavity design.

RF design

This section discusses details of the RF design of the shape of main Linac cavity.

Design philosophy The shape of a multi-cell SRF cavity is defined by a large number of parameters, which can be adjusted according to the design goals of the specific accelerator. In the case of the ERL, the cavity design needs to fulfill the following requirements:

- The RF design should reduce dynamic losses by the fundamental mode as far as possible while still satisfying the other design goals.

Table 2.4.4: ERL main Linac cavity design parameters. Note that R/Q is always in the circuit definition.

Parameter	Value
Type of accelerating structure	Standing wave
Accelerating mode	$TM_{0,1,0}$ π
Fundamental frequency	1.3 GHz
Design gradient	16.2 MV/m
Intrinsic quality factor	$> 2 \times 10^{10}$
Loaded quality factor	6.5×10^7
Cavity half bandwidth at $Q_L = 6.5 \times 10^7$	10 Hz
Operating temperature	1.8 K
Number of cells	7
Active length	0.81 m
Cell-to-cell coupling (fundamental mode)	2.2%
Iris diameter center cell / end cells	36 mm / 36 mm
Beam tube diameter	110 mm
Geometry factor (fundamental mode)	$270.7\,\Omega$
R/Q (fundamental mode)	$387\,\Omega$
$E_{\mathrm{peak}}/E_{\mathrm{acc}}$ (fundamental mode)	2.06
$H_{\mathrm{peak}}/E_{\mathrm{acc}}$ (fundamental mode)	41.96 Oe/(MV/m)
$\Delta f/\Delta L$	350 Hz/ μm
Lorentz-force detuning constant	1 Hz / $(MeV/m)^2$
Cavity total longitudinal loss factor for $\sigma = 0.6\,\mathrm{mm}$	14.7 V/pc
Cavity longitudinal loss factor for $\sigma = 0.6\,\mathrm{mm}$, non-fundamental	13.1 V/pC
Cavity transverse loss factor for $\sigma = 0.6\,\mathrm{mm}$	13.7 V/pC/m

- The RF design needs to support operation of the ERL at a 100 mA accelerating beam current.

- The performance of the RF design needs to be stable under small shape imperfections, which are unavoidable in the fabrication process of deep drawing and welding.

- The ratio of peak electric surface field to accelerating field $E_{\mathrm{pk}}/E_{\mathrm{acc}}$ shall not exceed 2.1 to reduce the risk of field emission (the ratio of electric fields in the ILC cavity is 2.0).

- The cell shape shall be non-reentrant. This simplifies cavity cleaning and surface treatment.

- Transverse kick fields in the coupler region shall be minimized to avoid emittance growth.

The RF design of the cavity is complicated by the fact that there are a large number of free parameters in the cavity shape and that there are different objectives for the design, which are partly contradictory because optimization for minimal losses and for maximal HOM damping

Table 2.4.5: Comparison of figures of merit and geometries for center cells before and after re-optimization to increase the width of HOM passbands. Cryogenic losses are slightly increased. The geometry factor and $E_{\mathrm{pk}}/E_{\mathrm{acc}}$ are for the fundamental mode. Key: Equ.=Equator, Horiz.= Horizontal, Vert.=Vertical. The last four dimensions are half-axes of ellipses, measured in cm.

	$(R/Q)G$	$E_{\mathrm{pk}}/E_{\mathrm{acc}}$	Wall angle	Iris radius	Equ. horiz.	Equ. vert.	Iris horiz.	Iris. vert.
Before	$15576\,\Omega$	2.00	85	3.5	4.399	3.506	1.253	2.095
After	$14837\,\Omega$	2.06	77	3.598	4.135	3.557	1.235	2.114

lead to different shapes of the cells. In designing the ERL main Linac cavity, the following approach has been taken to reduce the number of free parameters in each step by breaking the design work down into several steps, each focusing on a specific design objective:

- The center cells of the multi-cell main Linac cavity are identical and have been optimized initially to minimize dynamic wall losses by the RF field while keeping $E_{\mathrm{pk}}/E_{\mathrm{acc}} < 2.1$.

- The end cells were optimized to reduce the strength of the strongest dipole HOMs to increase the beam break-up (BBU) current above the design goal of 100 mA.

- The design was then evaluated for robustness under small shape imperfections and the shape of the center and end cells was iterated slightly to achieve sufficient robustness.

- The maximum number of cells was found by adding additional center cells to the multi-cell cavity design, and the BBU performance of the resulting cavity was simulated.

- The loss factor of the final cavity shape was computed and the input coupler region at one of the two end beam tubes was designed.

Center cell design   The center cells of the ERL main Linac cavity are identical and have been optimized initially to minimize dynamic losses while keeping $E_{\mathrm{pk}}/E_{\mathrm{acc}} < 2.1$. The shape of the cell was optimized for different iris radii between 30 and 43 mm (see Fig. 2.4.6 using a computerized optimization routine and the electromagnetic eigenmode code CLANS [16]. In each case, the shape dependent factor GR/Q was maximized to minimize the dynamic wall losses of the accelerating mode at a given field gradient. The usual basic cell shape consisting of two elliptical sections connected by a tangential line was used to ensure avoidance of multipacting in the cells.

Reducing the iris radius reduces the dynamic heat load by the RF field in the cavity, but increases the magnitude of the loss factor of the cavity. An increase in loss factors means an increase in average HOM power excited by the electron beam. Further, reduction of the radius reduces the cell to cell coupling and thus coupling of the HOM power to the beamline loads and the robustness of the design against small manufacturing errors. As discussed in [17], the parameter set resulting from the indicated compromises are presented in Tables 2.4.5 and 2.4.6.
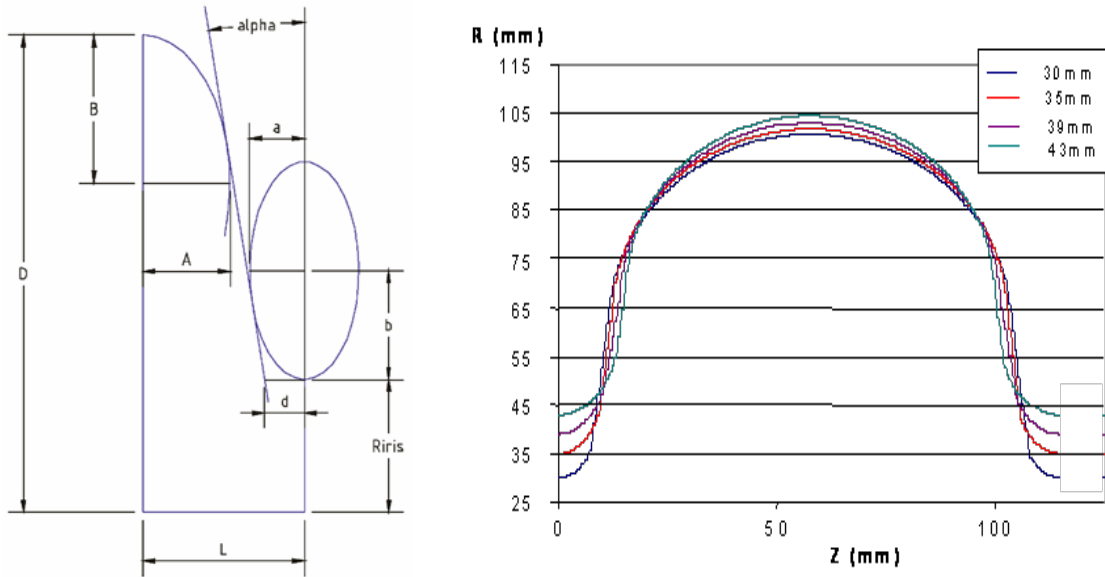
Figure 2.4.6: Left: Basic cell shape consisting out of two elliptical arc sections connected by a tangential straight line. Right: Center cell shaped for different iris radii optimized to minimize cryogenic losses (via maximizing GR/Q for the accelerating mode). The angle alpha of the tangential line is kept above 8° to ensure non-reentrant cell shapes.

End cell design and HOM performance   The ERL is specified to run accelerating currents of 100 mA through the main Linac. This current is limited by higher-order-modes in the cavity that are excited by the beam and can cause beam instability. In a 1-turn ERL, the threshold current I_{th}, through an isolated cavity with a single HOM, has been modeled as

$$I_{\text{th}} = -\frac{\omega_\lambda}{e \left(\frac{R}{Q}\right)_\lambda Q_\lambda} \frac{1}{T_{12} \sin(\omega_\lambda t_{\text{r}})} \, , \tag{2.4.5}$$

where ω_λ is the HOM frequency, Q_λ is the quality factor of the mode, R/Q is in units of Ω/cm^2 (in circuit definition), t_r is the bunch return time, and the transport matrix element T_{12} describes how a transverse momentum is transported to a transverse displacement after one turn [18]. Equation 2.4.5 suggests that the parameter $(R/Q)Q/\omega$ should be used as a

Table 2.4.6: Frequency width of the first 6 dipole passbands. Note that bands 3 and 6 were widened significantly while the other bands had their widths decreased only slightly.

Dipole band	$\sim 1.8\,\text{GHz}$	$\sim 1.9\,\text{GHz}$	$\sim 2.5\,\text{GHz}$	$\sim 2.7\,\text{GHz}$	$\sim 3.1\,\text{GHz}$	$\sim 3.4\,\text{GHz}$
Before	192 MHz	95 MHz	31 MHz	277 MHz	55 MHz	10 MHz
After	188 MHz	73 MHz	107 MHz	227 MHz	47 MHz	20 MHz
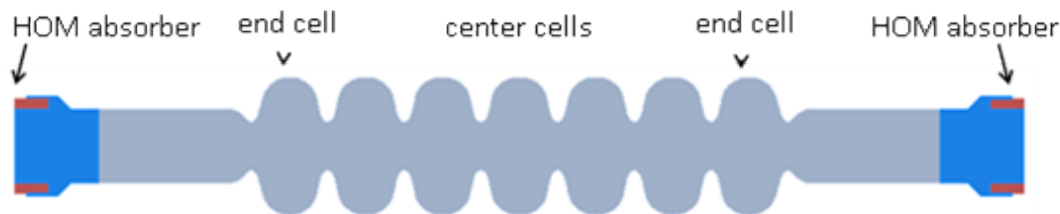
Figure 2.4.7: Shape of the main Linac cavity with HOM absorber sections at the beam tube ends.

figure of merit in the cavity design when optimizing it for maximal BBU threshold current. However, the ERL main Linac will have a large number of cavities, and coherent effects will influence I_{th} through the Linac. This coherent effect will depend on the variation of the HOM frequencies from cavity to cavity and on the quality factor of a given type of mode. Lower quality factors will result in wider HOM-resonance curves and therefore in more overlapping of the modes in different cavities, more coherence, and a lower threshold current. Thus, a new BBU figure of merit parameter was determined for an ERL Linac with a large number of cavities by running BBU simulations and varying the parameters of a given HOM in the cavities. The conclusion of the BBU runs is that

$$I_{\text{th}} \propto \frac{\omega_\lambda}{\left(\frac{R}{Q}\right)_\lambda \sqrt{Q_\lambda}} \qquad (2.4.6)$$

for an ERL Linac with a large number of cavities and for $10^2 < Q < 10^6$.

Accordingly, the end-cells of the ERL main Linac have been optimized with the goal to minimize the maximum value $(R/Q)_\lambda \sqrt{Q_\lambda}/f$ of any dipole HOM of the cavity. The end cells were optimized by varying 5 free parameters per end cell. The dipole mode fields and their damping were calculated with the 2D finite element codes CLANS2 [19] for HOM frequencies up to 10 GHz. The 2D-cavity model used is shown in Fig. 2.4.7, and includes the cavity itself, and half of an HOM absorber at either end (the center of an HOM absorber is the symmetry plane for a string of main Linac cavities). This model therefore simulates the Q in a string of cavities. The model includes the dielectric losses by the selected RF absorbing material in the HOM absorbers ($\epsilon' = 30$; $\epsilon'' = 20$; $\mu' = 1$; $\mu'' = 0$). Particle tracking was then used to compute the final threshold current through an ERL composed of these cavities. The blue curve in Fig. 2.4.8 shows that as the relative cavity-to-cavity HOM frequency spread increases, so does the threshold beam current. In practice, the frequency spread will be the result of slight variation in cavity shapes in the cavity fabrication process. This is shown as the red curve in Fig. 2.4.8.

Typical fabrication tolerances of ± 0.25 mm to ± 0.5 mm result in a cavity-to-cavity frequency spread σ_f/f of about 1×10^{-3} to 3×10^{-3}. At this frequency spread, particle tracking for the optimized 7-cell cavity predicts a BBU threshold current of about 300 mA to 500 mA, several times the 100 mA requirement for the accelerating beam of the ERL. If needed, the BBU threshold can be increased considerably by intentional means. An ensemble of cavity designs giving an approximately uniform frequency spread to the important HOM dipole bands will be created for the manufacture of the ERL cavities.
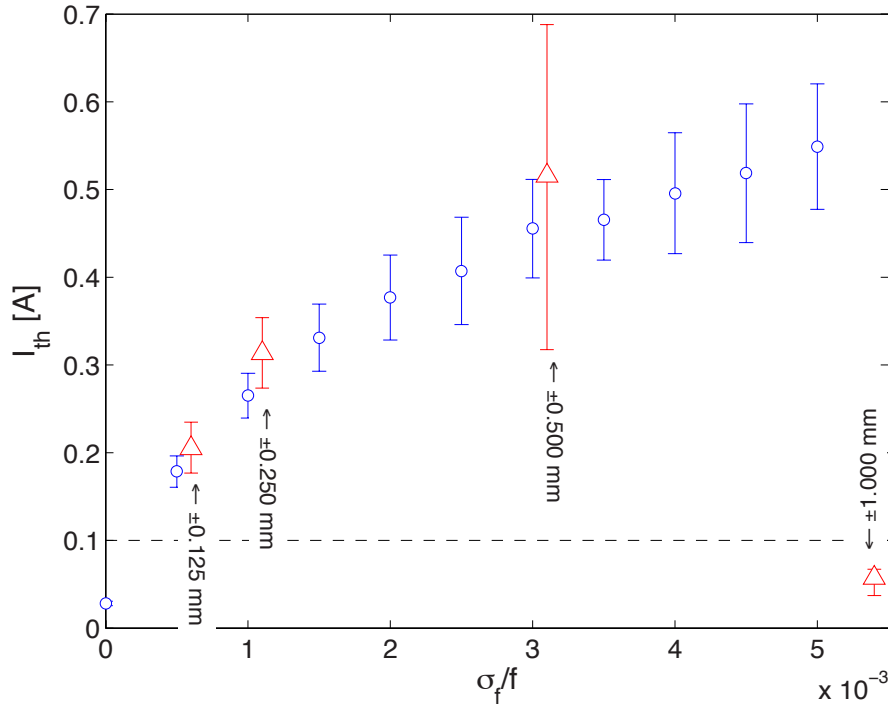
Figure 2.4.8: Average beam breakup current versus relative frequency spread for simulated ERLs. The blue circles mark the threshold current through an ERL with every cavity having the same nominal HOM frequency, Q, and R/Q values of the worst higher-order modes as a function of relative cavity-to-cavity frequency spread. The red triangles denote the average threshold current for ERLs generated from realistically shaped cavities, having different frequencies, Qs and R/Qs from shape imperfections, and no artificial cavity-to-cavity frequency spread. The lower (upper) error bars mark the threshold current that 90% (10%) of the simulated ERLs achieve. For small values, as machining tolerances loosen, the frequencies of cavity HOMs are spread over a larger range, contributing to larger threshold currents. When the machining errors are more than 0.5 mm, the underlying properties of the optimized cavity geometry are lost, and the threshold current plummets. In all cases except the 1 mm variation size, simulated ERLs well exceed the design specification of 100 mA current, denoted by the dashed horizontal line.
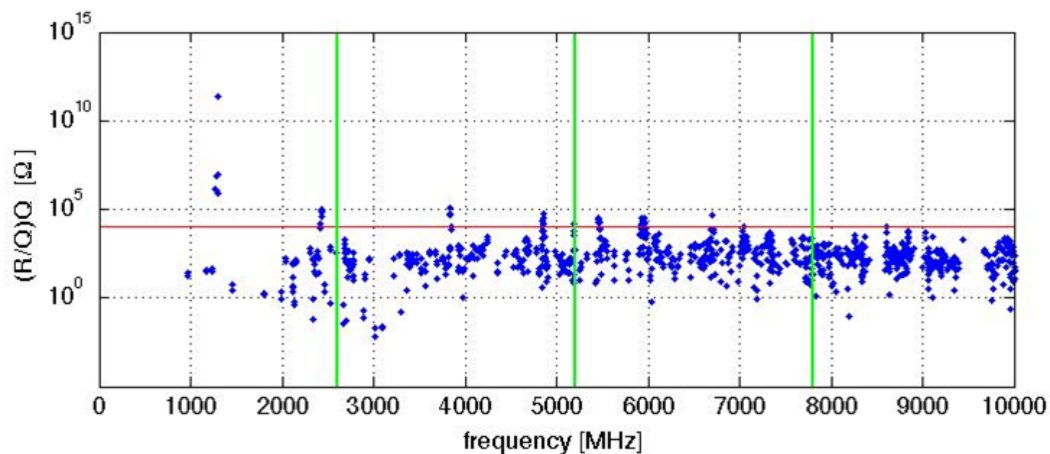
Figure 2.4.9: Monopole modes strength $(R/Q)Q$ for all monopole modes in the optimized 7-cell cavity up to 10 GHz. Green lines indicate the beam harmonics. The red line shows the $(R/Q)Q = 1000\,\Omega$ limit for modes within $\Delta f = 10^{-3} \cdot f$ of these harmonics. Modes with $(R/Q)Q > 1000\,\Omega$ that are not close the the green lines are benign.

All monopole modes up to 10 GHz have been calculated for the Linac cavity shape to ensure that modes that might be driven resonantly are sufficiently damped. The HOM power transferred to a mode by the beam in case of resonant excitation is given by

$$P = 2\left(\frac{R}{Q}\right)QI^2\,, \tag{2.4.7}$$

where Q is the quality factor of the mode and I is the average beam current (0.2 A for the combined accelerated and decelerated beam in the main Linac). Requiring that the maximum HOM power in case of resonant excitation is below 400 W per cavity then gives $(R/Q)Q < 10^4$ for any mode that could be excited resonantly, i.e. which has a frequency within $\Delta f = 10^{-3} \times f$ of a beam harmonic at $f = N \times 2.6\,\mathrm{GHz}$. Calculation shows that all monopole modes near the first 3 beam harmonics are sufficiently damped in the 7-cell ERL main Linac cavity. These results are shown in Fig. 2.4.9.

Short range wakefields The longitudinal loss factor $k_{||}$ of a cavity determines the average power transferred from the beam to electromagnetic fields (wakefields) excited by the beam,

$$P_{\mathrm{average}} = k_{||}qI\,, \tag{2.4.8}$$

where q is the bunch charge and I is the average beam current. The longitudinal loss factor and the wake potential of the 7-cell ERL main Linac cavity have been calculated for a bunch length of $\sigma = 0.6\,\mathrm{mm}$ yielding $k_{||} = 14.7\,\mathrm{V/pC}$, where the fundamental mode contributes 1.6 V/pC and the HOMs contribute 13.1 V/pC. Note that the main Linac cavities are one of the main contributors to the total impedance of the ERL and thereby make a significant contribution to the final intra-bunch energy spread . The average HOM power excited by the
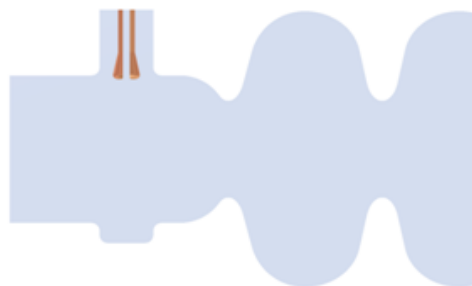
Figure 2.4.10: Input coupler port of the ERL main Linac cavity with $Q_{ext} = 6.5 \times 10^7$ and symmetrizing stub at the opposite site of the beam tube.

beam in a main Linac cavity is then about 200 W. Individual cavities will have smaller or larger power values, depending on their actual HOM frequencies (which will vary from cavity to cavity as a result of small cavity-shape imperfections), which will change the number of modes excited resonantly by the bunch train.

Input coupler port and transverse coupler kicks The position of the 40 mm input coupler port on one of the cavity end-beam tubes was found such that the tip of the inner conductor of the coax input coupler protrudes 2.7 mm inside of the beam tube wall at an external Q of 6.5×10^7 (see Fig. 2.4.10). Non-zero transverse fields can be present in the input coupler region even on the beam axis since the coupler port breaks the axial symmetry. Such transverse coupler fields are highly undesirable, since they will cause emittance growth of the beam passing the ERL main Linac. One way of reducing the emittance growth is adding a small symmetrizing stub across from the coupler as illustrated in Fig. 2.4.10. The stub is used to minimize the asymmetry in the beam pipe, causing the transverse fields in the coupler region. The method reduces amplitudes of the off-axis fields and thus reduces the magnitude of the coupler kick with weak dependence on the depth of the stub once it is over 10 mm deep [20]. Our preliminary design therefore uses 20 mm depth.

Mechanical design

This section gives an overview of the mechanical design of the Cornell ERL main Linac cavity, including its LHe vessel and inner magnetic shield.

Mechanical modes The cavity cells will be fabricated out of 3-mm thick Niobium sheets for mechanical strength, with stiffening rings between the individual cells. The optimal position of these stiffening rings will be found by mechanical simulations with ANSYS. The objectives of these optimizations are (1) to increase the resonance frequencies of mechanical vibration modes of the cavity to reduce cavity vibration excitation by external sources, and (2) to decrease the frequency shift of the accelerating mode by fluctuations in the LHe bath pressure surrounding the cavity. The power density of the ground vibration spectrum decreases with frequency so high mechanical resonance frequencies of the cavities are desirable to reduce driven vibrations. Figure 2.4.11 shows the lowest frequency mechanical vibration modes of

Stif. ring	0.7*r_{eq}	0.65*r_{eq}	0.4*r_{eq}	no ring
mode	freq / Hz	freq / Hz	freq / Hz	freq / Hz
1	131.03	115.15	85.34	54.62
2	131.04	115.15	85.33	54.62
3	315.52	268.39	191.3	133.34
4	315.52	268.39	191.3	133.34
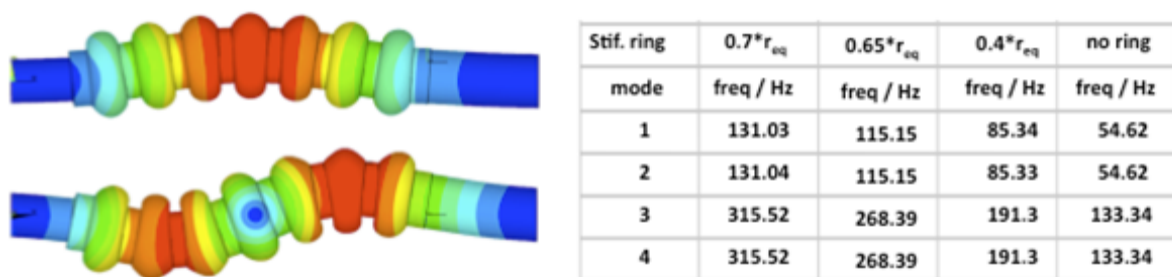
Figure 2.4.11: Mechanical vibration modes of the main Linac 7-cell cavity for different radial positions of the stiffening between the individual cells. r_{eq} is the cell equator radius.

the main Linac cavity structure for different radial positions of the stiffening rings between the cells. As expected, the frequencies of the modes increase with the radial position of the stiffening rings. An upper limit for the radial position is given by the requirement that the cavity needs to remain tunable in length by the frequency tuner, and by the second objective that the sensitivity to LHe pressure changes should be minimized.

As the example in Fig. 2.4.11 shows, the radial position of the stiffening rings also changes the sensitivity of the cavity frequency to fluctuations in the pressure of the liquid helium surrounding the cavity cells. Optimizing the position of the rings allows minimizing this contribution to the cavity microphonics.

The beam tubes of the main Linac cavity will be fabricated out of 1.5 mm thick, low-RRR niobium to reduce static heat loads from the HOM absorbers located between the cavities at 100 K to the 1.8 K cavities.

Cavity flanges Different types of flanges have been used on superconducting cavities in the past, including niobium flanges with indium wires, ConFlat-flanges, and aluminum diamond shaped gaskets with NbTi flanges. The main objective of these flanges is to provide a clean, highly reliable connection to the next element in the beamline. However, in high current accelerators like the ERL, it is also crucial that the impedance of the flange design be as small as possible to eliminate potential heating issues, since they are inside the cryomodule vacuum and therefore cooled only via conduction through the beam-pipe.

KEK has developed a zero-gap (zero-impedance) flange design, which uses a copper gasket compressed between two small, flat surface rings with 90° edges [21] (see Fig. 2.4.12). NbTi versions of such a zero-gap flange design will be considered for use in the ERL main Linac for the cavity flanges. An R&D program has been started to verify the high reliability of this flange design found in previous studies [22]. In parallel, a new flange design will be studied which is a hybrid of the KEK zero-gap [21], a DESY diamond seal [22] and a taper seal flange [23]. This configuration shown in Fig. 2.4.13 may allow for the reliability of the DESY diamond seal with low compression force and elastic spring as well as the minimal wall perturbation of the KEK zero-gap.
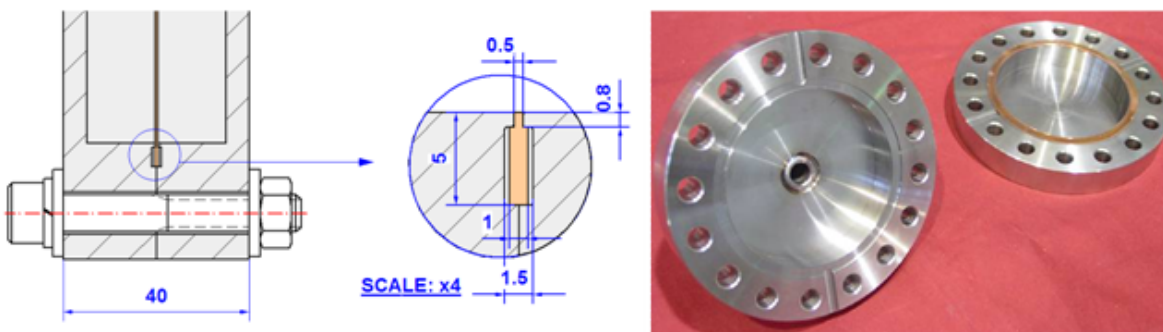
Figure 2.4.12: Zero-gap KEK flange design [23].
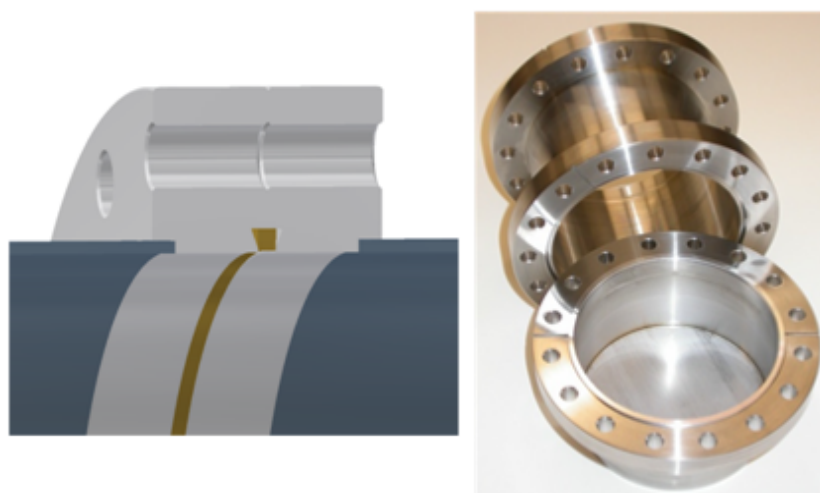
Figure 2.4.13: Vacuum flange hybrid of the KEK zero-gap, a DESY diamond seal and a taper seal flange.

LHe vessel   The cavity cells are welded into a cylindrical titanium vessel, which holds the superfluid helium needed for cooling the cavities to 1.8 K. The tank further serves as part of the cavity-frequency tuning system, including a short bellow section to allow the length of the cavity to be adjusted, and is used to support the cavity in the cryomodule. Titanium has a thermal contraction which is almost identical to that of niobium, thereby minimizing any buildup of mechanical stresses during cool-down of the cavity from room temperature to 1.8 K. A stainless steel vessel would have a 2 times larger thermal contraction than the niobium cavity and would result in intolerable stresses in the cavity, resulting in plastic deformation unless the tuning mechanism is operated during cool-down. Titanium has the additional advantage that it can be welded directly to the Nb/Nb-Ti conical vessel end plates on the cavities using either TIG welding or electron-beam welding.

The heat flux (power per cross-sectional area) through superfluid helium in the LHe vessel needs to be less than the limiting heat flux of $\sim 1.5\,\mathrm{W/cm^2}$, at which the temperature of the bath at the heat source would reach the lambda point, and the helium would cease to be superfluid. The smallest cross-sectional areas of the helium in the tank surrounding the cavity
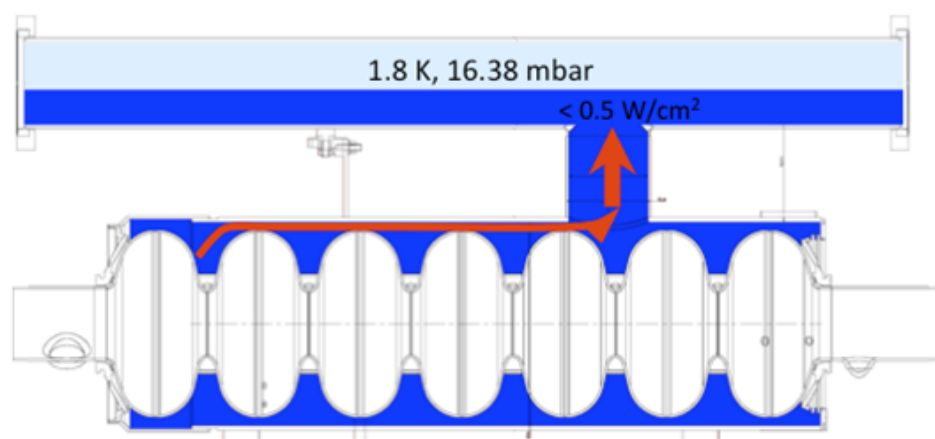
Figure 2.4.14: Heat flow in the LHe vessel and the chimney connecting the tank to the two phase line. The heat flow in the superfluid helium is below $0.5\,\mathrm{W/cm^2}$ everywhere.

are at the cell equators (see Fig. 2.4.14). The diameter of the LHe vessel has been chosen such that the heat flux in these areas stays well below $1.5\ \mathrm{W/cm^2}$ at the chosen operating parameters.

During initial cool-down, the LHe vessels of the cavities can be filled via a warm-up - cool-down pipe connected to the bottom of the LHe tanks. A chimney of sufficiently large diameter $(> 20\,\mathrm{cm^2})$ connects each LHe tank to the two-phase He pipe in the cryomodules as shown in Fig. 2.4.14.

The cavity-helium tank structure is a mechanical structure with many eigenmodes driven by external vibration sources and pressure fluctuations the LHe bath. The mechanical design of this structure is optimized to avoid low-frequency mechanical resonances and resonances at multiples of the 60 Hz line frequency to minimize cavity microphonics. Measurements at the Cornell ERL injector cryomodule have shown that the dominating source of microphonics is due to fast fluctuations in the LHe pressure [24]. The stiffness of the cavity-helium tank structure is therefore designed to minimize the frequency shift of the cavity with changes in LHe pressure.

Inner magnetic shield It has been shown that a DC residual magnetic flux present at the cavity will be trapped when the cavity is cooled through the transition temperature. This results in a residual resistance of about $0.35\,\mathrm{n\Omega}$ per mG of trapped flux at 1.3 GHz [25]. The earth's field must be adequately shielded to achieve high Q_0 factors. The residual DC-magnetic field at the cavity locations needs to be much less than 30 mG to achieve residual resistances below $10\,\mathrm{n\Omega}$ and intrinsic quality factors above 2×10^{10} at 1.8 K. In the ERL, this will be achieved by three layers of shielding of the Earth's magnetic field: an outer vacuum vessel made out of carbon-steel, an outer magnetic shield at room temperature lining the inside of the vacuum vessel, and an inner magnetic shield around the LHe vessels of the cavities. The inner shield will be made out of A4K, [26], which has a high permeability at cryogenic temperatures, and will be heat treated for operation at 2 K. The shielding design goal is $< 2\,\mathrm{mG}$.
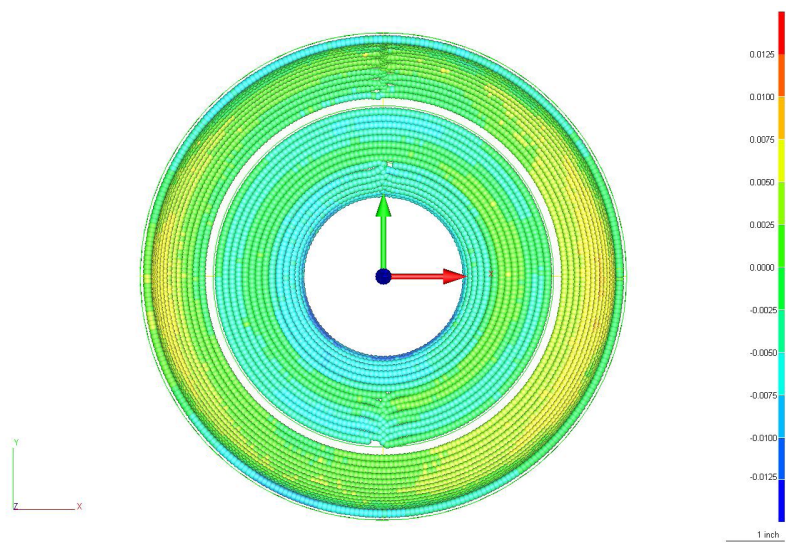
Figure 2.4.15: Overall accuracy of the cavity cup shape, measured with a coordinate-measuring machine. The deviation from the ideal shape is well below 200 μm, being better than required by the BBU limit estimated above.

Table 2.4.7: Summarized target frequencies for all cavity production steps.

Production Step	Frequency (MHz)
Cavity designed shape in vacuum	1299.655
Cavity designed shape in air	1299.234
Cavity nominal desired freq as built	1298.985
Air, 20C, 150 μm BCP	1297.425
Vacuum, 20 C	1297.884
Vacuum, 2 K	1299.700
Vacuum, 2 K, tuned 300 kHz (stretched)	1300.000

Cavity fabrication

The ERL main Linac cavities will be fabricated from high-purity (RRR > 300) bulk niobium. RRR 300 Niobium has become the standard in SRF cavity fabrication, with higher RRR values often produced by post-purifying the cavity at around 1400° C. This improves the thermal conductivity of the material, which in turn safeguards against quenches due to normal-conducting defects. An eddy-current scan or newer techniques based on SQUID scans of the delivered sheets will be used to detect such defects in the niobium before it is used for cavity production. The half cells for the cavities are deep-drawn and then electron-beam welded to fabricate the full 7-cell cavity. As shape variations play an important role in determining the BBU limit, a careful analysis of all pressed cups is essential. Our data on 7 prototyped cavity showed the maximum deviation being less than 200 μm. Figure 2.4.15 shows a typical measurement, taken with a coordinate-measuring machine (CMM).
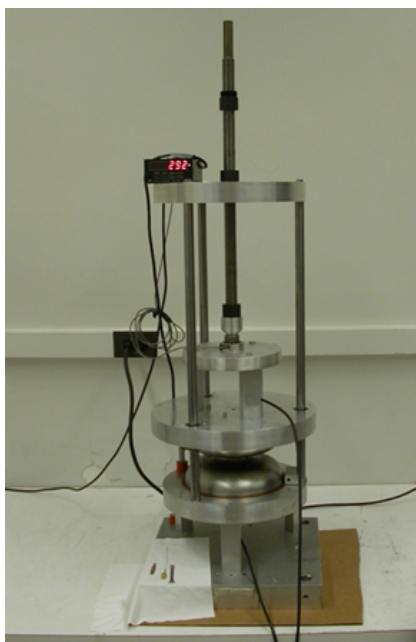
Figure 2.4.16: RF measurement set-up to determine the dumbbell trimming. This individual trimming process ensures a proper compensation of the small shape variations, leading to an almost perfect cavity after all fabrication steps

After pressing the cups, two of them are welded at the iris to form dumbbells. These dumbbells have excessive length at the equator and trimmed individually to account weld shrinkage, chemical etching, and cooling to 1.8 K. Table 2.4.7 summarizes the different frequencies targeted during the production steps, ensuring that the cavity will have the correct frequency at its operating temperature. The trimming length for the dumbbells is determined by an RF measurement, shown in Fig. 2.4.16.

After trimming the dumbbells, the full cavity is welded together. The beam-tube sections are of extruded, low RRR-niobium tubes, with NbTi flanges (ratio 45/55 by weight) electron-beam welded to them.

The field flatness of a cavity fabricated in that manner is shown in Fig. 2.4.17. Even though the field flatness (as a result of the dumbbell trimming) is pretty good, the whole cavity is tuned to field flatness after the chemistry process again. The apparatus to do this is also shown in Fig. 2.4.17. The procedure described above is suitable for a large series production have been developed and transferred to industry before [27].

Cavity treatment

Numerous techniques for cavity surface preparation exist [28]. These include an initial degrease, chemical etching with BCP (HF, HNO_3 and H_3PO_4, usually in a ratio of 1:1:1 or 1:1:2) or electropolishing, followed by high-pressure water rinsing, and heat treatments at 600 to 1400° C for hydrogen degassing or post purification, respectively. These steps may have to be repeated several times. A final treatment often includes in-situ baking at around 120° C
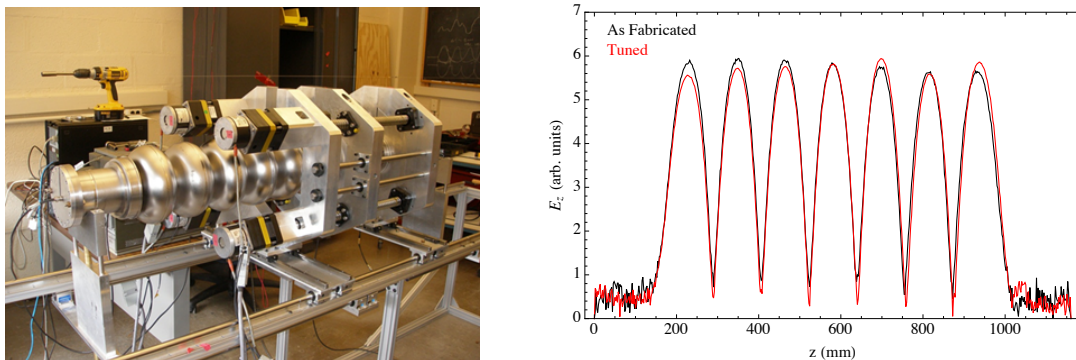
Figure 2.4.17: Left: This setup is used to tune each cavity to a flat field. It slightly pushes or pulls on the irises, while the field flatness is measured with a bead-pull.
Right: Measured field flatness of a cavity as welded and after field flatness tuning, measured with a bead-pull set-up.

for 48 hours, which has been shown to improve the BCS losses and often removes the so-called "high-field Q-slope" that frequently limits the cavity performance [29].

It is desirable to simplify the treatment of the ERL main Linac cavities as much as possible while still meeting the performance specifications. Chemical etching with BCP has been shown to reliably yield accelerating gradients of 20 to 25 MV/m in multi-cell cavities [30]. Following fabrication of the cavity, a "damage layer" of 100 to 200 μm will be removed from the inner cavity surface in several steps by BCP to achieve good RF performance. This removal is taken into account in the cavity design. The acid is cooled below 15° C during the process to minimize hydrogen migration into the niobium. After high pressure rinsing with ultra-pure water and drying in a class 10 clean room, the cavities will be annealed at 800° C in an ultra-high-vacuum furnace to out-gas hydrogen and relieve mechanical stress built up during the cavity-fabrication process. This heating step is followed by tuning the individual cavity cells for field homogeneity of the accelerating mode and a second, light BCP (~ 10 μm). In the final step the cavities will be high pressure rinsed again, evacuated and heated at 120° C for 48 hours to minimize the BCS surface resistance. The performance of the cavities will be verified in an RF vertical acceptance test in a superfluid helium bath cryostat.

Current research indicates that electropolishing might result in higher intrinsic quality factors at medium field gradients [31] and thereby compensate for the added cost and complexity of electropolishing. If future research confirms this, one or both of the BCP steps in the ERL cavity preparation might be replaced by electropolishing.

2.4.3 Tuner

The function of the tuner is to stretch or compress the SRF cavity along its beam axis to adjust the frequency of the accelerating π-mode at 1.3 GHz. This adjustment is needed to synchronize the resonant frequencies of all 384 cavities in the Linac to the master oscillator.

As part of the tuner-cavity mechanical system, the cavity's cylindrical helium tank will incorporate a short bellows section to minimize the tank's longitudinal mechanical stiffness,

leaving only the stiffness of the niobium cavity cells for the tuner to act upon. The tuner is attached to the helium tank with attachment points that span the tank's bellows. Thus nearly all of the tuner components must operate at the helium tank temperature of 1.8 K.

Two different operating regimes are required of the tuner. First, a slow time-scale response of the order 1 Hz with a coarse-cavity tuning range of $\sim 600\,\text{kHz}$ is needed to adjust the cavity frequency due to influences such as:

- contractions upon cooldown to 1.8 K

- variations in helium bath pressure

- manufacturing irregularities

- de-tuning a problematic cavity to minimize beam interaction.

Slow tuning is typically accomplished by a stepping motor with gearing and levers to provide the requisite force along the cavity axis. The slow portion of the tuner is utilized after cavity cooldown to adjust the frequency operating point, and exercised rarely thereafter until warmup. The cavity must be parked in a specific state of compression by the slow tuner prior to cooldown from 293 K to 1.8 K so that the differential thermal contraction between the tuner and the cavity does not plastically deform the cavity. The same requirement for the parked condition applies during warm-up.

The second tuning regime is a fast time-scale response of the order of 1 kHz with a fine cavity tuning range of ~ 1 kHz. The fast tuning is needed to adjust the cavity frequency due to influences such as:

- Lorentz force detuning during cavity field ramp up

- correction of microphonic perturbations of the cavity

- feedback control within the low-level RF system to adjust beam-transit phase,

Fast tuning is accomplished by sandwiching piezo-electric ceramic stacks between the slow tuning mechanical linkages and their cavity attachment locations. The actuated piezo force/displacement then adds in series to the slow-tuning mechanism to result in a superposition of the forces upon the cavity. The piezos must be rated for an adequate blocking force and elongation given a reasonable actuation voltage in the cryomodule vacuum insulation environment. The piezo actuation voltage should be less than 1000 V at maximum displacement for reliable wiring within the vacuum vessel. Listed in Tab. 2.4.8 are the performance parameters required for both the fast and slow components of the ERL Linac SRF cavity tuner.

Design of the main Linac cavity tuner

Several proven options are available for the cavity-tuner design. The choice for the baseline tuner was between adaptations of the Saclay I tuner [32–34] and the INFN-blade tuner [35], related to earlier work at DESY. Both designs have performed well in SRF cavity tests at various facilities and have experienced several generations of optimization, but both designs

Table 2.4.8: ERL Linac cavity tuner performance specifications.

Parameter	Value
Cavity elongation tuning	$350\,\text{Hz}/\mu\text{m}$
Cavity spring constant	$4.63 \times 10^6\,\text{N/m}$
Cavity force tuning	$289\,\text{Hz/N}$
Cavity lowest mechanical resonance	$91\,\text{Hz}$
Slow tuner response bandwidth	$1\,\text{Hz}$
Slow tuner cavity frequency range	$600\,\text{kHz}$
Slow tuner dimensional range	$368\,\mu\text{m}$
Fast tuner response bandwidth	$1\,\text{kHz}$
Fast tuner cavity frequency range	$1.5\,\text{kHz}$
Fast tuner dimensional range	$0.9\,\mu\text{m}$
Minimum piezo blocking force	$2073\,\text{N}$
Maximum piezo voltage	$1000\,\text{V}$
Minimum tuner spring constant	$6 \times 10^9\,\text{N/m}$
Minimum tuner mechanical resonance	$1000\,\text{Hz}$
Tuner operating temperature	$1.8\,\text{K}$

require modest modifications for the ERL Linac application. The Saclay I tuner was chosen for the ERL Linac due to the following features that are advantageous to CW, high Q_{ext} cavity operation:

- lower group delay in its tuning response, resulting in lower phase lag for microphonic compensation [36, 37]

- more compact, making integration of the magnetic shield simpler

- mechanically simpler, reducing manufacturing and assembly cost

- greater reliability statistics given its use in the FLASH facility

Also, since the Saclay tuner will be used in the XFEL facility presently under construction, a foundation of production testing and industrial experience will be established.

An illustration and photograph of the Saclay I tuner is shown in Fig. 2.4.18. The modifications to the tuner in Figure Fig. 2.4.18 will be to increase the bore diameter to fit over a larger diameter beam tube of the 7-cell cavity and to select a piezo stack matched to the tuning forces of the cavity.

2.4.4 HOM load

The Higher Order Mode (HOM) loads in the cryomodule are intimately linked to the SRF cavity design and mitigation of the beam breakup instability (BBU) as described in §2.4.2. The average HOM power is expected to be 200 W per cavity. Most of the power will be in the frequency range 1-10 GHz, but the short ERL bunch length will allow HOM spectral content up to the 100 GHz range. The HOM damping scheme must then have strong coupling over
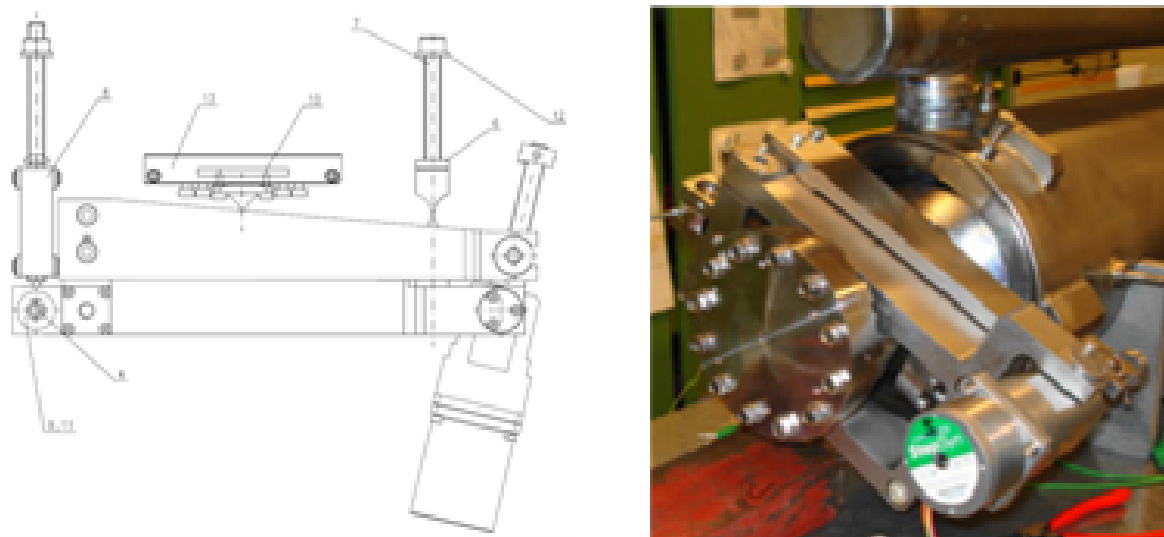
Figure 2.4.18: Illustration and photograph of the a Saclay I tuner.

this broad bandwidth and be able to dissipate the high average power. Among the options for an HOM damping configuration are:

- beamline loads where the RF absorber is a lining of the beampipe

- loop-coupled antenna located in side apertures on the beampipe that absorb HOM power at 2–5 K or transport RF in coax to remote loads

- waveguide loads coupled transversely to the beampipe that transport the RF to remote loads

- button-type pickups located in small apertures on the beampipe that transport RF in coax to remote loads.

The beamline loads are conceptually straightforward, where HOMs propagate as TE or TM modes in the circular beampipe and are heavily damped at the absorber. This provides broadband damping with only modest dependence on the RF absorber properties and no need for careful geometrical tuning of coupling structures. To avoid an undue load on the refrigeration plant from the expected 200 W of HOM power, the RF absorber is maintained at 100 K and thus necessitates thermal gradients along the beamline between cavities. The thermal gradient is defined by a 5 K intercept between the 1.8 K cavity and the 100 K HOM absorber, where selection of the 100 K temperature was a result of an optimization process to minimize the total cryogenic load of the full module as described in §2.4.8 below.

The challenge with beamline loads is that since the RF absorber resides on the beamline, only tens of centimeters from the SRF cavity, in addition to RF absorption it must also be: high vacuum compatible, have finite DC conductivity to drain static charge, be able to withstand significant radiation, have no particulate generation, and have the requisite thermo-mechanical properties to operate at cryogenic temperatures as configured in an HOM- load assembly.

Such beamline loads have performed well at room temperature as part of the CESR-B [38] and KEK-B [39] cryomodules for over a decade. A cryogenic version of a beamline load was installed in the ERL injector prototype cryomodule [40] and valuable insight was gained from the cold tests and beam operation. In the HOM prototypes, it was discovered that all three types of RF absorbing materials have their DC conductivity drop at cryogenic temperatures, and can thus accumulate considerable static charge and deflect low energy beams [41]. Also, thermal expansion differences between the RF absorbers and their heat sinks can result in long-term fatigue than can eventually cause solder bonds to delaminate. This insight has guided development of a next-generation beamline load that resolves these issues as described in §2.4.4 below. A cryogenic version of a beamline load has also been developed for the XFEL cryomodule [1] and has been shown to perform well in that application, although its power limit of about 100 W may not be sufficient for the ERL Linac.

Loop-coupled HOM loads are prevalent on several SRF cavity designs, such as XFEL, ILC, and SNS [42, 43]. In these pulsed-beam applications, the average absorbed HOM power is only a few watts. Much larger powers were absorbed in the HERA electron ring with 50 mA beam current. There have nevertheless been challenges revealed with loop couplers in operating machines, such as with antenna overheating, multipactor, and mis-tuning due to fabrication variations [44] [45]. The button-type HOM couplers are still at the conceptual and modeling stage of their development, and it is expected that they will face bandwidth, power, and tuning challenges analogous to those of the loop couplers. A challenge with the modeling and analysis of loop and button-HOM damping is that they have non-axisymmetric geometries and require 3D-simulation tools. The meshing and computational demands then become time consuming and can restrict the number of modes and accuracy of the analysis, raising the concern that a BBU susceptible HOM could be missed, especially with component fabrication variations [46].

Waveguide-HOM couplers have been successfully used at JLAB for many years at lower powers, typically around 10 W [47].

The use of waveguide-HOM coupling is the subject of ongoing investigations [5], and while they could have the benefit of transporting the HOM power to external room-temperature loads, it is still to be determined if they will have the requisite damping bandwidth, and how the full structural complexity will compare to that of beamline loads.

Beamline-HOM loads have been chosen for the baseline Cornell ERL main Linac design to best accomplish the damping requirements that are critical to mitigating BBU. Details of their design are presented in the following sections.

ERL main linac HOM load

A CAD model of the ERL main Linac beamline HOM load is shown in Fig. 2.4.19. The load has an RF absorber as a unitary cylinder brazed into a tungsten-heat sink, stainless-steel bellows for flexibility of flange alignment and cavity length variations. There will be 5 K intercepts at the transition between the bellow and the end-group section, the later will be copper plated to avoid excessive RF heating. The HOM load will be mounted to the Helium Gas Return Pipe (HGRP) as well.

RF-absorbing materials that have the requisite properties are in advanced development and full scale samples are in hand. They are based on SiC or AlN with embed carbon nanotubes or graphite. A key is to have a sufficient fractional loading of carbon so as to exceed the
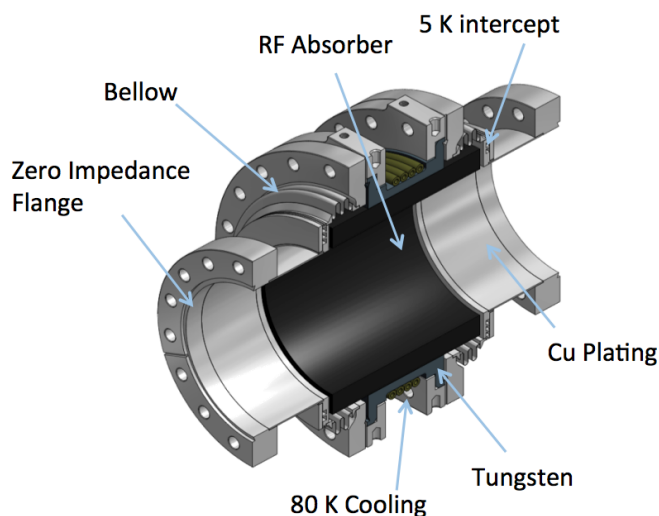
Figure 2.4.19: CAD model cross section of the ERL main Linac beamline HOM load.

percolation threshold in the material and establish a DC conductivity that is nearly independent of temperature. This will also provide a satisfactory broadband dielectric loss tangent of $\delta = 0.2 - 0.6$. Plots of measured RF and DC electrical properties of a carbon- loaded RF absorbing ceramic are shown in Fig. 2.4.20. This material appears to satisfy all of the electrical and particulate requirements of a beamline HOM load absorber [48]. First in situ tests show adequate RF absorption, while the DC conductivity may slightly differ from batch to batch.

For the HTC program, two prototype HOM absorbers have been fabricated (see Fig. 2.4.21 showing the HOM absorber installed under the HGRP and connected to the cavity). Based on this prototype experience some optimization is currently underway. This is mainly dedicated to get reliable batch to batch material properties and to accommodate for the rather low CTE of the material. As a cost saving measure, the material can be shrink-fitted to Titanium which we successfully proved on a sample cylinder.

2.4.5 Input coupler

The fundamental RF-input coupler has two main functions: i) efficient transfer of power from an RF power source to the accelerating mode of a beam-loaded RF cavity, i.e., a passive impedance matching network, and ii) providing an RF-transparent barrier between a gas-filled transmission line, coaxial or waveguide, and the ultra-high vacuum of the beamline RF cavity, which necessitates the use of at least one ceramic RF window.

Several CW and pulsed RF-power couplers have been developed at different laboratories around the world for superconducting cavities, both rectangular waveguide and coaxial configurations [49]. Since the ERL superconducting Linac cryomodule is based on TTF technology, early on in the project we decided [50] to use coaxial couplers derived from the TTF-III design [51, 52]. This input coupler has the following important features:

- Low static heat leak
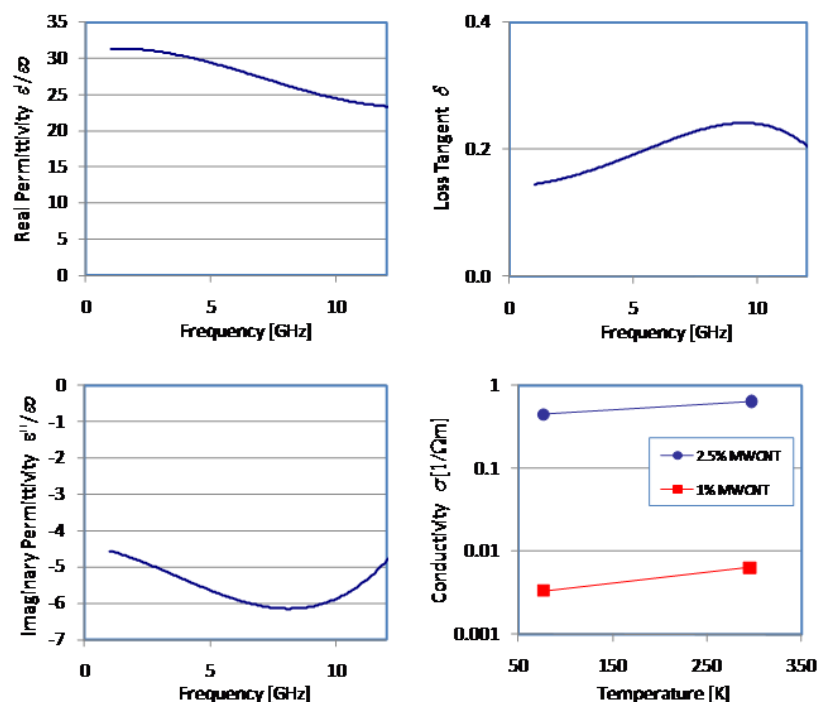
Figure 2.4.20: Measured RF and DC electrical properties of a carbon-loaded RF absorbing ceramic.

- Two ceramic windows - one warm and one cold - allowing sealing of the SRF cavity input coupler port during an early assembly stage in a clean room, thus reducing the risk of cavity contamination

- Coupling to the cavity adjustable over one order of magnitude by varying the axial position of the inner-conductor antenna

- Bellows accommodating lateral movement of the cavity in a cryomodule by up to 15 mm during cool-down from room temperature to 2 K

The TTF-III coupler was designed for a pulsed superconducting Linac application. Hence not all of the features of the TTF-III design are relevant for the ERL main Linac, which operates CW with 2/5 kW CW average/peak power. Further, there are features specific to CW operation that must be added to the TTF-III design. A wealth of experience in designing, fabricating, testing, and successfully commissioning CW RF couplers has been gained for the prototype-ERL injector, described in §2.3.6. Here we describe a conceptual design for the ERL main Linac RF coupler.

ERL main Linac coupler design

The input couplers for Cornell Energy Recovery Linac must deliver up to 5 kW CW RF power to the main Linac cavities, though under nominal conditions they will operate with 2 kW
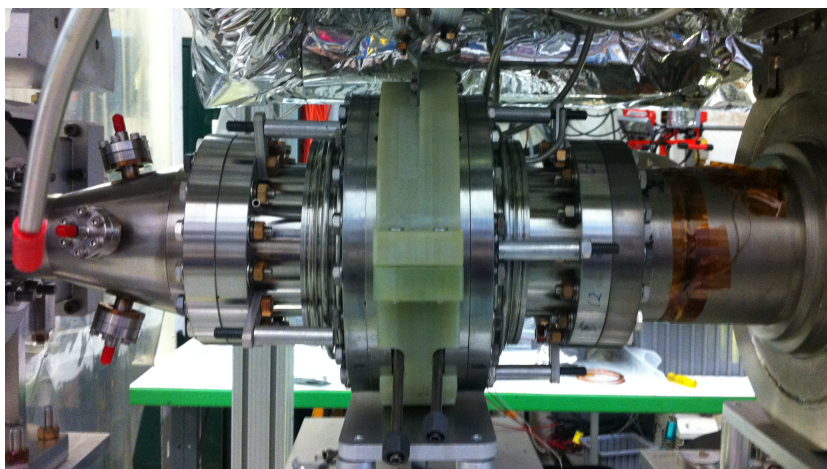
Figure 2.4.21: HOM absorber installed under the HGRP within the HTC cold mass

average and 5 kW peak power. The 5 kW peak power is required for transient modulation to compensate for cavity detuning due to microphonic perturbations. Due to the principles of energy recovery in a superconducting cavity, the couplers will operate under conditions with full reflection for the great majority of the time and thus require active cooling of the inner conductor as in the ERL injector input couplers. To make the design more economical, the couplers will provide fixed coupling to the cavities with $Q_{\text{ext}} = 2 \times 10^7$ Coupling adjustability can be achieved using three-stub tuners in the feed-transmission line to have a range of $2 \times 10^7 - 1 \times 10^8$, with the nominal operational $Q_{\text{ext}} = 6.5 \times 10^7$.

The design of the ERL main Linac coupler takes into account experience gained from the ERL injector couplers [53]. The proposed main Linac coupler is shown in Fig. 2.4.22 and Fig. 2.4.23 [54]. This design utilizes a rectangular-waveguide-feed transmission line, though it is possible that a coaxial-feed line could be implemented to reduce space if it is compatible with the design of the full RF-power delivery system. As with the TTF-III and ERL-injector couplers, the ERL main Linac coupler consists of three sub-assemblies: the cold and warm coaxial sub-assemblies, and the waveguide. The two coaxial portions of the coupler and their ceramic windows are the same size as those in the TTF-III coupler. The cold portion of the coupler with the protruding antenna attaches to the SRF-cavity coupler-port flange, which will be at a temperature slightly above 2 K. A copper thermal intercept held at 5 K is located on the coupler outer conductor a few cm from the cavity flange to minimize the heat load to the 1.8 K-cavity helium vessel. An 8" ConFlat flange then joins the cold coupler to the warm coupler. The warm coupler has two bellows sections on both the inner and outer conductors for flexible compliance, as will be described in the next paragraph. The warm coupler has a copper thermal intercept held at 100 K located on the outer conductor a few cm from the vacuum vessel flange to minimize the heat load to the 5 K system. The vacuum vessel flange resides at 293 K, beyond which is a vacuum pumping port on the outer conductor for the warm portion of the coupler, an instrumentation port, and then the coax-rectangular waveguide transition. All coaxial components, with the exception of the inner-conductor antenna portion and the thermal intercepts, are made of stainless steel with copper plating on surfaces carrying RF
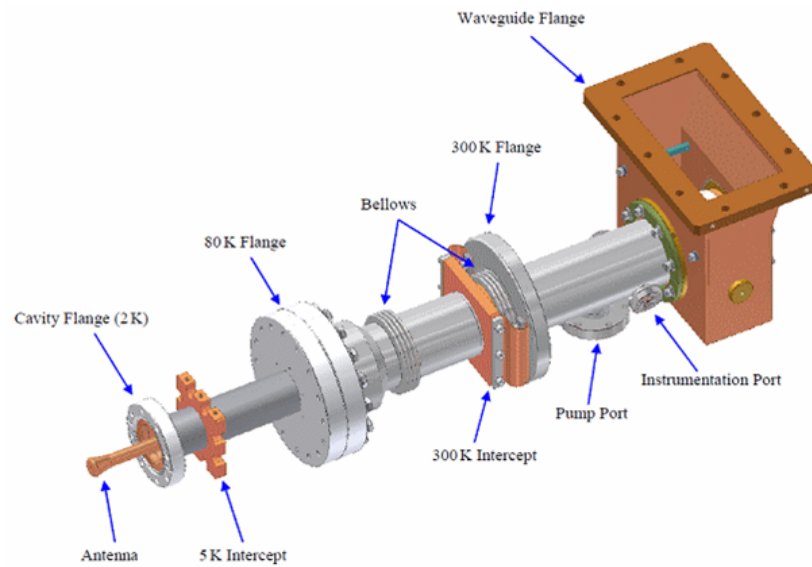
Figure 2.4.22: CAD model of the fully assembled ERL Linac input coupler.
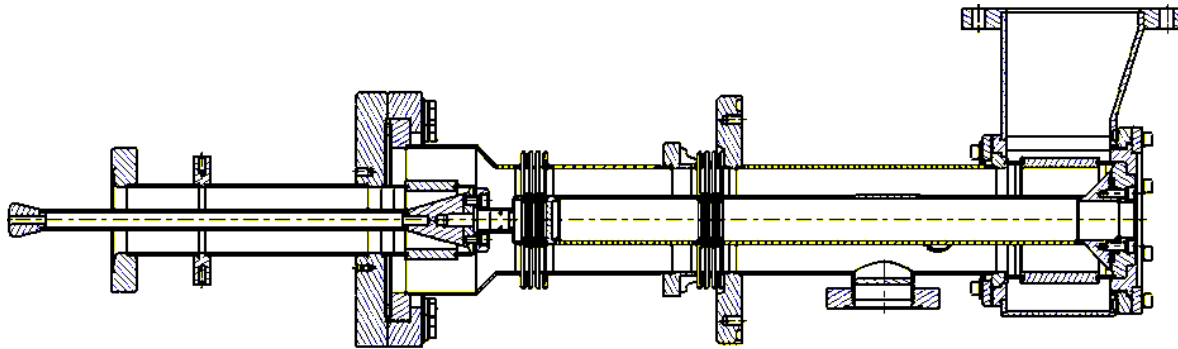
Figure 2.4.23: Section view of the ERL Linac input coupler.

currents.

Similar to the TTF-III couplers, the ERL Linac couplers must accommodate lateral movement of the cavities during cool-down of up to 10 mm, since one end of the coupler is attached to the moving cavity and the other end is attached to the fixed vacuum vessel port. For the TTF-III couplers, bellows on the inner and outer conductors of the warm assembly and on the outer conductor of the cold assembly provide some flexibility. This arrangement, however, causes the antenna to skew. If the lateral movement is large enough, the antenna can touch the outer conductor of the cavity coupler port. Besides shorting the coax coupler, the scratching of the surfaces will generate copious particulate and significantly degrade the SRF-cavity performance. For the ERL Linac coupler, this problem is overcome by placing two sets of bellows only on the warm portion of the coupler, on both the inner conductor and on the outer conductor, as shown in Fig. 2.4.24. In this way, high flexibility is achieved while keeping the cold antenna fixed relative to the cavity coupler port.
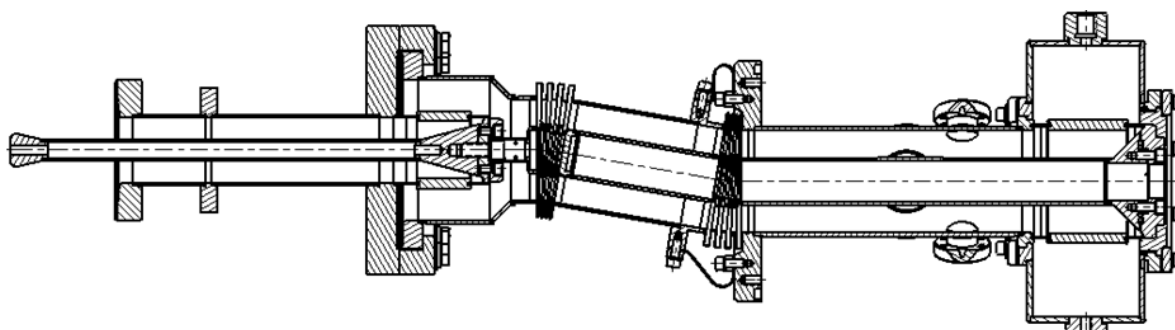
Figure 2.4.24: The ERL Linac input coupler is mechanically flexible, yet maintains alignment of the cavity antenna.

Table 2.4.9: Heat loads of the ERL main Linac input coupler.

	Static Heat Load	Dynamic Load at 2 kW CW
2 K	0.03 W	0.15 W
5 K	1.55 W	1.94 W
80 K	2.26 W	9.33 W

The static and dynamic heat loads of the ERL main Linac input coupler are listed in Tab. 2.4.9. The elimination of a thin-walled bellows on the cold sub-assembly to maintain a fixed antenna alignment slightly increases the static heat load to the 5K thermal intercept. However, this contribution to the total refrigeration load of a Linac cryomodule is a small percentage, as summarized in §2.4.8.

The ERL main Linac input coupler has been modeled for multipactor susceptibility using the code Mutipac2.1 [55]. The results showed no evidence of mutipacting in the ERL RF coupler.

2.4.6 Superconducting quadrupole and dipoles

Each Linac cryomodule contains one quadrupole with adjacent horizontal and vertical steering coils.

Quadrupole design

A iron yoke magnet design has been selected for the quadrupole since the relatively low gradient can be realized with a conventional iron-based design using superconducting coils, allowing the quadrupole to utilize the 1.8 K liquid helium available in the cryomodule. A CAD model of the yoke and coils is shown in Fig. 2.4.25, with the coils also shown separately for clarity. The pole pieces have a hyperbolic shape with a 70 mm bore and the coils lie flat except at the ends. The coils for this type of lens are single layered and can be manufactured with minimal effort [56]. Numerical simulations of the quadrupole were performed with MERMAID and take into account the real properties of the yoke material (Steel 1010). A detailed parameter
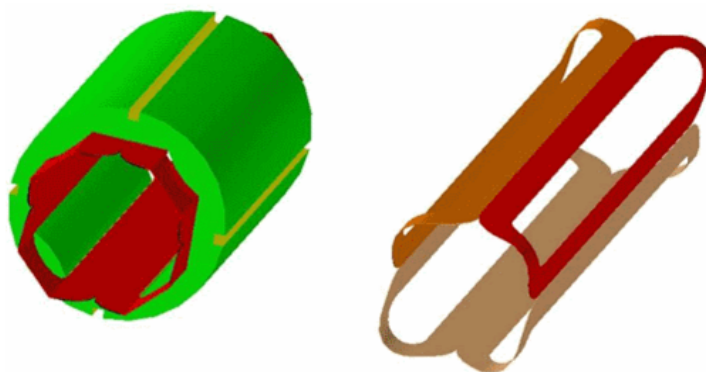
Figure 2.4.25: Isometric view of the quadrupole lens cold mass (at the left) and the set of four coils without the iron (at the right).
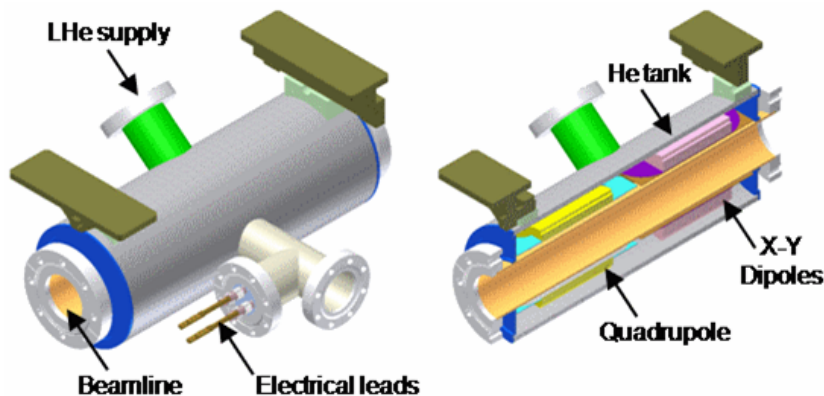
Figure 2.4.26: The superconducting quadrupole and dipole lenses in their helium vessel with the HTS leads.

list of the quadrupole is given in Tab. 2.4.10. A CAD model of the full quadrupole and dipole package is shown in Fig. 2.4.26. The length of the assembly is $\sim 350\,\mathrm{mm}$.

The stray magnetic field from the magnet package must be carefully minimized inside of the cryomodule to maintain a high SRF cavity Q_0. The typical background magnetic field inside of the module vacuum vessel will be about 25 mG, and additional shielding intimate to the SRF cavity will reduce this to $< 2\,\mathrm{mG}$ at the cavity walls. The amplitude of the unshielded quadrupole magnetic field along the beamline at a 1 cm radius is shown in Fig. 2.4.27. The field drops off rapidly, where at a distance of 15 cm from the edge of the yoke it is $< 3.7 \times 10^{-5}$ of its value at the center of the quadrupole, corresponding to a maximum unshielded stray field of $\sim 65\,\mathrm{mG}$. Cryogenic magnetic shielding will also be wrapped around the magnet package to ensure that the stray field is negligible.

Table 2.4.10: Parameters of the ERL main Linac superconducting quadrupole magnet.

Winding type	Flat coils
Iron yoke inner diameter	70 mm
Iron yoke outer diameter	107 mm
Maximal current	110 A
Maximal gradient	19.4 T/m
Linac module current range	$0.75 - 49$ A
Linac module gradient range	$0.13 - 8.6$ T/m
Magnetic length	125.6 mm
Number of turns	86/pole
Wire diameter (bare/insulated)	0.33/0.41 mm
Copper to superconductor ratio	2:1.66
RRR	> 100
Filament diameter	$20\,\mu$m
Twist pitch	25.4 mm
Iron yoke length	100 mm
Coil length	137 mm
Stored magnetic energy at max current 100 A	45 J
Self inductance	0.009 H
Integrated gradient at current 100 A	2.21 T
Integrated b6/b2 at current 100 A, at 30 mm	1.8×10^{-3}
Integrated b10/b2 at current 100 A, at 30 mm	2.7×10^{-3}
Coil peak field	0.76 T
Gradient at 2.5 A	0.00437 T/m
Saturation at nominal current 100 A (integrated)	0.17%

Dipole design

For the dipole corrector, a single-layer coil is chosen similar to that for the quadrupole. However, the dipole coil is placed inside of the iron yoke as this gives minimal stray fields outside of the corrector, as seen in Fig. 2.4.28 and Fig. 2.4.29. Again, numerical simulations of the dipole were performed with MERMAID and take into account the real properties of the yoke material (Steel 1010). A detailed parameter list of the dipole is given in Tab. 2.4.11. The stray magnetic field from the dipole does not decay as rapidly as for the quadrupole field, as seen in Fig. 2.4.29. The stray dipole field is still quite low, however, and the dipole will be located downstream of the quadrupole, away from the SRF cavity closest to the magnet package, so that it is adjacent to the gate valves, as shown in Fig. 2.4.2.

Installation in the cryomodule

The magnet package body will reside at the 1.8 K temperature of the helium vessel. The four HTS current leads coming out of the assembly will have a 5 K heat sink and then a 100 K heat sink at the module thermal shield. The four leads will be wired as:
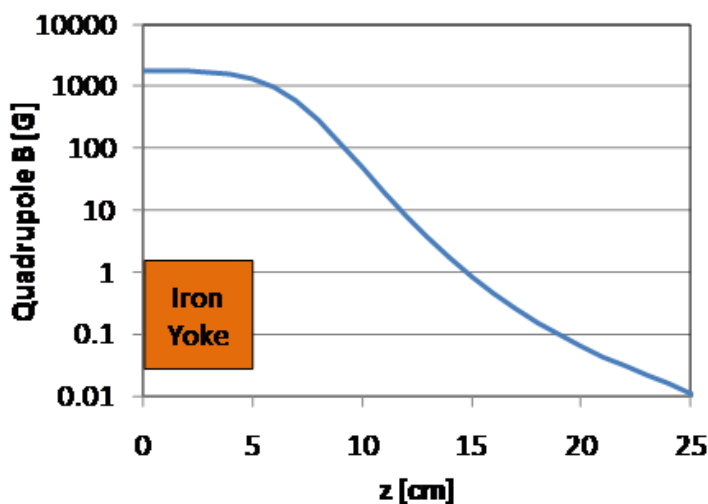
Figure 2.4.27: Unshielded quadrupole field dependence along the beamline at a 1 cm radius. The iron yoke ends at 5 cm.

1. Quadrupole supply

2. X-dipole supply

3. Y-dipole supply

4. Common return

The typical heat leak for a 200 A, 150 mm long HTS lead between 77 K to 4.2 K is 20 mW. So the total heat leak to 1.8 K could reach $0.08 - 0.1\,\mathrm{W}$/package. The HTS leads will also be wrapped by magnetic shielding to reduce their stray-magnetic fields. From this analysis, the heat load of the entire magnet system is negligible compared to the dynamic load of the cavities.
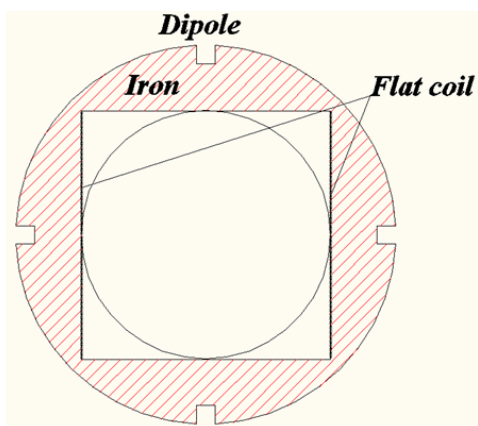
Figure 2.4.28: The dipole corrector superconducting coils and iron yoke.
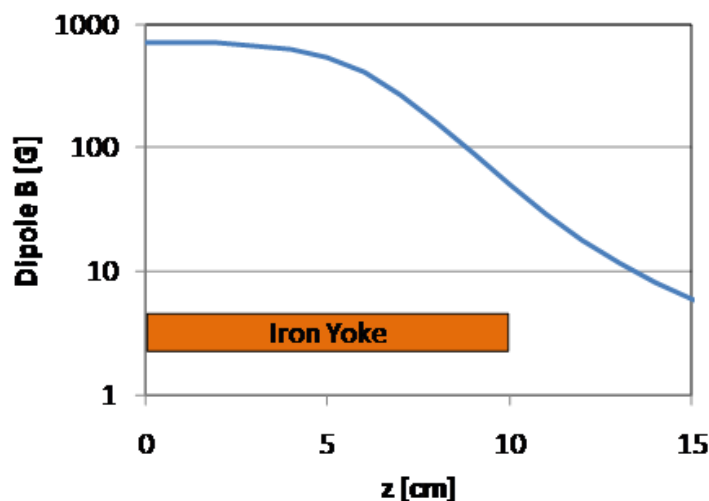
Figure 2.4.29: Unshielded dipole field dependence along the beam axis. The iron yoke ends at 10 cm.

2.4.7 Cryomodule beam position monitor

A beam position monitor (BPM) will be included in every main Linac cryomodule and will be located adjacent to the magnet package. The BPM will be held at a temperature of about 5 K. Under consideration are both a button-style BPM similar to that developed for the XFEL at DESY [57] and a compact design as used in CESR-TA. Both types are shown in Fig. 2.4.30.

2.4.8 Cryomodule

The ERL Linac cryomodule design is based on TTF-III technology with modifications for CW operation. In this technology scheme, the cryomodule units that are about 10 m long are connected by bellows with no intervening warm breaks, and all connected units share a common insulation vacuum. The cryogen transfer lines are internal to the module vacuum vessel and are connected between units in situ by welding together flexible joints. The beamline is also connected in situ between units under a portable clean room.

The ERL Linac cryomodule (shown in Fig. 2.4.2) is based on the TTF-III module structure. All of the cavity-helium vessels are pumped to 1.8 K (16 mbar) through a common 30 cm inside diameter Gas Return Pipe (HGRP), which also serves as the mechanical support from which the beamline components are suspended. To minimize the heat load to the refrigeration plant, all of the 1.8 K cryomodule components are surrounded by 5 K intercepts to minimize the heat leak to 1.8 K, and the 5 K intercepts are likewise surrounded by 100 K intercepts, which absorb the heat load from the 293 K vacuum vessel. The HGRP is suspended from composite support posts that are constructed from low-thermal conductivity G-10 fiberglass. The composite posts have integral metal stiffening disks and rings that also serve as thermal intercepts at 5 K and 100 K between the 1.8 K face that attaches to the HGRP and the 293 K face that attaches to the vacuum vessel bosses that support the cold mass. There are stainless steel manifolds of smaller diameter than the HGRP running the length of the modules that

Table 2.4.11: Parameters of the ERL main Linac superconducting dipole magnets.

Winding type	Flat coil
Yoke aperture square side	70 mm
Yoke outer diameter	107 mm
Maximal current	22 A
Maximal field	0.071 T
Typical current	11 A
Typical field	0.03 T
Magnetic length	138 mm
Number of turns	88
Wire diameter (bare/insulated)	0.33/0.41 mm
Copper to superconductor ratio	2:1.66
RRR	> 100
Filament diameter	20 m
Twist pitch	25.4 mm
Iron yoke length	100 mm
Coil length	170 mm
Stored magnetic energy at nominal current 20 A	1.4 J
Self inductance	0.007 H
Integrated b1 at nominal current 20 A	0.935 Tcm
Integrated b3/b1 at nominal current 20 A, at 30 mm	3.2×10^{-3}
Integrated b5/b1 at nominal current 20 A, at 30 mm	1.7×10^{-3}
Coil peak field	0.6 T
Saturation at nominal current 20 A (integrated)	0.1 %

transport the supply of liquid helium and the supply and return of 5 K and 100 K helium gas for the thermal intercepts. Jumper tubes with 5 mm inner diameter are connected between the 5 K and 100 K supply and return manifolds to the various thermal intercepts within a module. A shell of 6 mm thick, grade 1100 aluminum sheet surrounds the beamline and the HGRP and is linked to the 100 K manifold to serve as a thermal radiation shield between the 293 K vacuum vessel and the cold mass. The aluminum 100 K shield has apertures through which the RF couplers pass and also has panels with instrumentation feedthroughs. The 100 K shield is mechanically suspended from one of the integral metal stiffeners in the composite support posts. Multi-layer insulation is wrapped around the exterior of the 100 K shield as well as all of the 1.8 K and 5 K cold mass components.

As the full ERL main Linac is assembled in the tunnel, cryomodule units are brought into place, the beamlines are aligned, and a flexible joint connected under a portable clean room then mates the beamline module-to-module. The cryogenic manifolds are welded together with short bellows sections as well as the HGRP. A short section of 100 K shield is inserted between modules to maintain its continuity and a flexible sleeve adapter then joins the adjacent vacuum vessels.

The magnetic shielding in the cryomodule must keep the field in the region of the cavities to $< 2\,\mathrm{mG}$ to have negligible residual wall loss and provide a good safety margin for the goal of

(a) Similar to XFEL (b) Compact CESR-TA
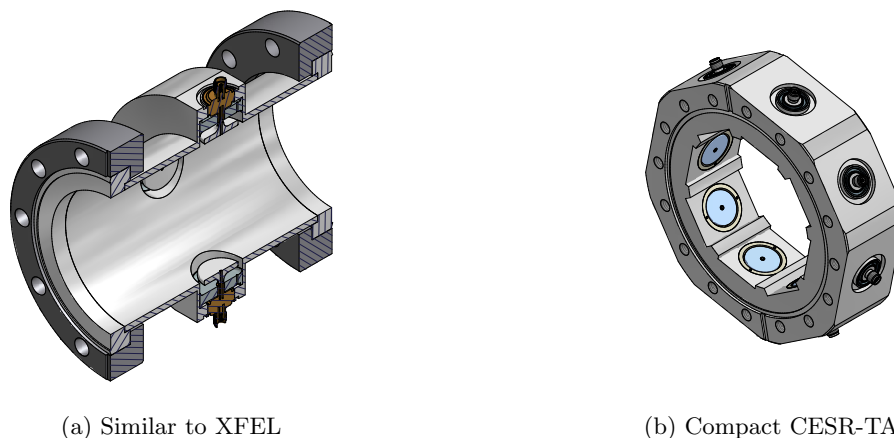
Figure 2.4.30: Linac BPM designs.

cavity $Q_0 = 2 \times 10^{10}$. Such a low field is accomplished by de-gaussing the carbon steel vacuum vessel, lining it with co-netic mu-metal shielding that will be at 293 K, and then wrapping each cavity's 1.8 K helium vessel with a magnetic shield that is formulated to have maximal shielding at low temperatures around 4 K [58].

ERL Linac modifications to TTF-III technology

The CW, high current operation of the ERL Linac necessitates several changes to standard TTF technology which has evolved for low-duty factor operation. Additional changes unrelated to CW operation have been implemented here as a result of experience gained from fabrication and operation of TTF modules. Most of these changes were also implemented in the ERL injector prototype cryomodule, as described in §2.3.6, and have proven to be successful [59]. Briefly, the main differences between the ERL Linac cryomodule and the TTF-III module are:

- Implement beamline HOM loads for strong broadband damping of HOMs generated by the high current and short bunches.

- Use a high average power coax RF input coupler per cavity, with lateral flexibility for cool down and fixed coupling. Detailed modeling and appropriate cooling for the prototype ERL injector have shown that overheating can be avoided.

- Do not include a 5 K shield

- Increase the diameter of the cavity helium vessel port to 10 cm for the high CW heat load

- Include a JT valve in each cryomodule for the high CW heat load.

- Increase the diameter of the 2-phase 2K He pipe to 10 cm for the high CW gas load.

- Use precision fixed surfaces between the beamline components and the HGRP for easy "self" alignment of the beamline

- Use rails mounted on the inside of the vacuum vessel and rollers on the composite support posts to insert the cold mass into the vacuum vessel, as opposed to the "Big Bertha" handler

- Cooling of thermal intercepts is provided by small "jumper" tubes with flowing He gas, such as to the HOM loads and the RF couplers, as opposed to copper straps

- Locate access ports in the vacuum vessel to allow the tuner stepper motor to be accessible for replacement while the string is in cryomodule

Cryomodule beamline components and lengths

The ERL Linac cryomodule length is chosen as a balance between beam optics considerations and keeping the unit physically manageable. The maximum module length for transport on a standard flat-bed truck is about 16 m or 52 ft. To maximize the Linac's active acceleration fill factor, it is desirable to place quadrupoles as sparsely as possible. Beam optics simulations show that the maximum quadrupole spacing is about one doublet every twelve 7-cell cavities. This would give a cryomodule length of about 19 m, which is too long. The fill factor can be maintained while shortening the module length by having six cavities with one quadrupole and one set of horizontal and vertical corrector coils per module. Thus the quadrupole doublet is accomplished in every two modules with a manageable module length of 9.82 m or 32.2 ft. Listed in Tab. 2.4.12 are the ERL main Linac cryomodule beamline components, their individual lengths, and the total length of the module.

Cryomodule components and assembly

Cryomodule assembly starts with the beamline and proceeds as a layered growth out to the vacuum vessel and warm coupler attachment. The specific choices for the configuration of many of the components also impacts the configuration of other components. For example, the choice between using a blade tuner vs. a Saclay tuner dictates the type of bellows and support flanges on the cavity helium vessel, as well as the permalloy magnetic shield around the helium vessel. Similarly, the choice of the required power rating of the coupler significantly alters not only the complexity of the coupler, but also the details of the vacuum vessel coupler ports, such as their dimensional and alignment error tolerance, which is a cost driver. Described in the following is the assembly sequence of the baseline choices for the principle cryomodule components, along with descriptions of the components not discussed in previous sections.

Beamline string assembly

The beamline consisting of the cavities, HOM loads, cold couplers, quadrupole, steering coils, beam position monitor, tapers, and gate valves (Tab. 2.4.12) is assembled in a class 100 or better clean room. All components are flushed with filtered water or alcohol and individually receive a mild vacuum bake at $120°\,C$ for 24 hours. The components are mounted on an assembly fixture one by one in the clean room. Each added component is aligned to the other components with the only critical alignment being the azimuthal position about the beam axis. This azimuthal alignment is needed so that the flat precision mounting surface at their tops

Figure 2.4.31: Cryogenic and RF rated pneumatic gate valves for the beamline.

will mate to the planar-precision surfaces on the HGRP. This alignment can be accomplished with a simple accurate spirit level. Any longitudinal spacing or planar shift errors of the mounting surfaces is accommodated by the flex in the HOM load bellows. The component mating vacuum flanges are then bolted together. A photograph of the assembled ERL injector prototype beamline string in the clean room is shown in Fig. 2.3.34. After all components are attached, the string is vacuum leak tested while still in the clean room so that only filtered particulate-free air will pass through any potential leak. The pumping and purging during the leak test is performed at a slow rate of 1-2 Torr/minute through the viscous flow range of 760 Torr to 1 Torr to minimize propagation of any particulate contamination throughout the beamline.

A beamline component not described in previous sections is the gate valve. To maintain the cleanliness of the beamline, the gate valves at each end of the string must be closed after the vacuum-leak test in the cleanroom and rarely opened again until the cryomodule is installed in its final tunnel location. A cryogenic-rated gate valve is available from VAT, which also has an "RF aperture" to provide RF shielding in the open position for accelerator beamline service. A photograph of this valve is shown in Fig. 2.4.31. This valve was also designed to have a demountable pneumatic actuator that includes a vacuum vessel flange. With this feature, the cold mass can be inserted into the vacuum vessel without the actuator, then have the actuator attached through a vacuum vessel port with the controls and pneumatic connections available exterior to the vacuum vessel. The Linac interlock control system can then seal off any cryomodule in the event of a vacuum trip. A photograph of the valve installed in the ERL-injector prototype vacuum vessel is shown in Fig. 2.4.32. The addition of a pneumatic actuator differs from the gate valves used in TTF modules where the valve is only manually operated, is inaccessible from the vacuum vessel exterior, and is opened just prior to sealing the vacuum vessel joint between modules with no possible automated interlock closure.

Cold mass assembly fixture and HGRP attachment

As a parallel operation to the beamline string assembly in a clean room, the cold mass assembly fixture can be set up in a high-bay area with overhead crane access. The composite support posts are attached to the HGRP and the HGRP is hung from the assembly fixture by the composite posts. The 2-phase pipe is then mounted aside the HGRP using G-10 standoffs and its exhaust is welded into the HGRP. A photograph of the ERL Injector HGRP hung from
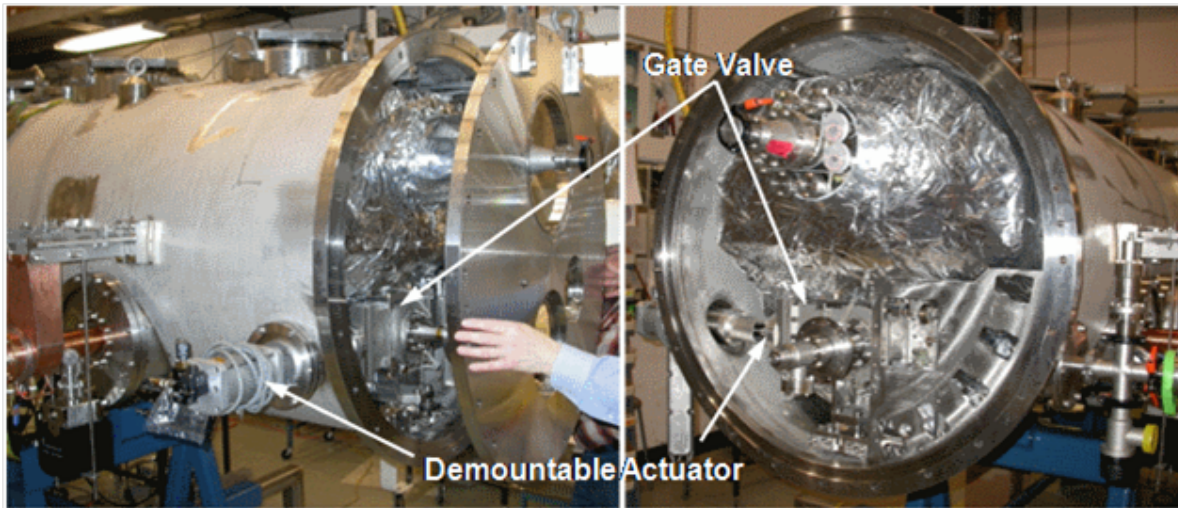
Figure 2.4.32: Cryogenic-rated pneumatic gate valve installed in the ERL Injector vacuum vessel.

the cold mass assembly fixture by the composite posts is shown in Fig. 2.4.33.

The choice of the number of composite posts supporting the HGRP and the HGRP wall thickness were determined by analyses of the static deformation of the titanium HGRP due to the estimated 4082 kg (9000 lb) weight of the cold mass and by the desire to lessen the relative motion of beamline components due to thermal contraction. The result was a decision to employ four posts per cryomodule with two sections to the HGRP. A schedule 80 pipe section was selected for the HGRP. With these choices the resulting static deflection is computed to be 0.07 mm with peak stress of 17 MPa providing a large safety factor compared to the 275 MPa yield published for Grade 2 Ti.

Beamline string attachment to HGRP

After the beamline string passes the vacuum leak test, it is removed from the clean room and positioned underneath the cold mass assembly fixture. The string is raised and the precision mounting surfaces on the string and the HGRP are brought together with integral alignment pins and keys being engaged. The mating surfaces are then bolted together. String attachment to the HGRP in this manner proved to be quick and easy for the ERL injector, the entire procedure taking about 1 hour. Shown in Fig. 2.4.34 is the injector beamline hung from the HGRP.

Cavity magnetic shielding and tuner

After the beamline is hung from the HGRP, the helium tanks of the cavities are wrapped with magnetic shielding. This shielding will reside at 1.8 K. Consequently, this magnetic shielding layer is fabricated from A4K [58], which retains its shielding properties at cryogenic temperatures.
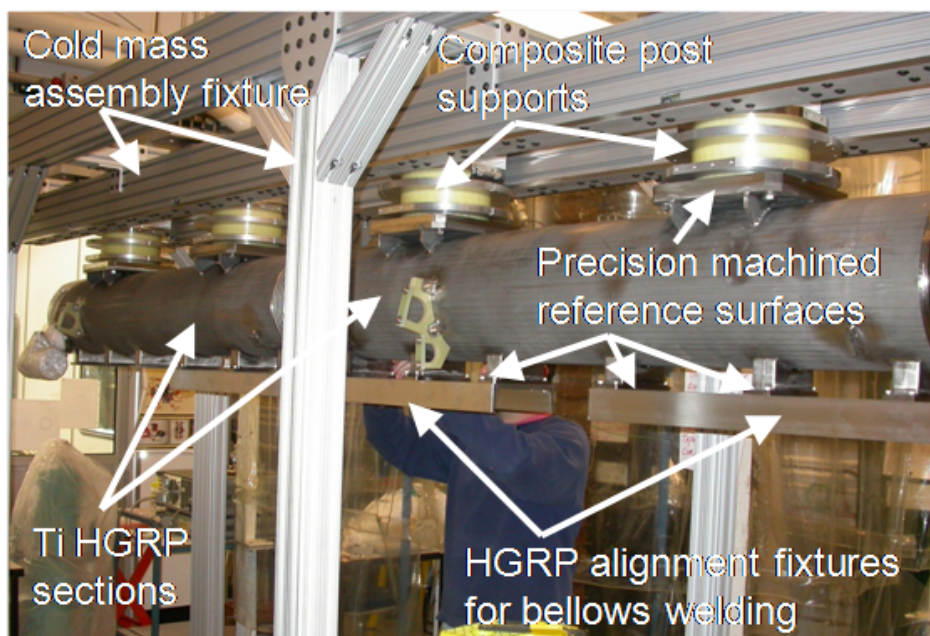
Figure 2.4.33: HGRP and 2-phase pipe hung from the cold mass assembly fixture by the composite posts for the ERL Injector.

The cavity tuners are attached after the magnetic shielding. The stepping motors of the tuners have to be wrapped in a copper sleeve that is tied to 5 K line to prevent the motor heat from propagating to the helium vessel. The stepping motors are also wrapped with A4K shielding since they can have stray fields of a few hundred milliGauss in close proximity to access apertures in the cavity shield. Part of the tuner attachment process is pre-bias of the tuner force on the cavity. This bias is required to compensate for stresses developed during cooldown due to CTE differences between the cavity materials and the tuner materials. Without the pre-bias force, it is possible that the cavity could plastically deform, the piezos could crack, or the piezos could become loose, depending on the specific configuration of the tuner. A good measure of the bias force is the frequency of the cavity at room temperature. The tuner is initially attached with the cavity in its relaxed position. Then Belleville washers in the piezo support mechanism are compressed with adjustment nuts until the cavity is at its target biased warm frequency. Note that the beamline cold couplers have protective caps placed on them in the clean room, and the caps include a spring-loaded RF contact from the coupler center conductor to an SMA header on the cap. This allows the cavity frequency to be monitored during the tuner bias operation. A photograph of the tuner bias operation for the ERL injector is shown in Fig. 2.4.35.

Liquid He, 5 K gas manifolds and thermal intercepts

Several cryogen manifolds run the length of the cryomodule and are welded to those of the next module during module installation in the Linac tunnel. These manifolds include a liquid helium supply to the JT valve required per module, a liquid helium supply to the "warm-

Figure 2.4.34: Beamline string hung from the HGRP for the ERL Injector.

up/cool-down" ports located at the bottoms of the helium vessels needed for convective flow, the supply and return of 5 K helium gas, and the supply and return of 100 K helium gas. A JT valve is required per module due to the high cavity heat load and helium mass flow for CW operation.

The liquid helium and 5 K gas manifolds are mounted close to the HGRP using G-10 standoffs, thus keeping similar temperatures in close proximity to each other with low thermal conductivity connections between them. These manifolds are the next components mounted on the cold mass. Jumper tubes from the liquid helium manifolds are then routed to the JT valve and the helium vessel fill ports. The 5 K gas supply and return manifolds must then be routed to thermal intercepts on the HOM loads and RF couplers by way of jumper tubes having 3-5 mm ID. In standard TTF technology, the connections between the manifolds and thermal intercepts are accomplished by copper straps. For the ERL Linac, both the 5 K and 100 K heat loads are large enough to require gas flow from the manifolds to the intercepts through jumper tubes. If high RRR copper or aluminum straps were used as heat sinks, the cross-sectional area would be tens of cm^2 and consume too much space, as well as not being sufficiently flexible. Flexible straps made of "tough pitch" copper attached between the 5 K manifold and the composite support post 5 K rings provide sufficient thermal conductance for this intercept.

100 K manifolds and thermal shield

The 100 K manifolds are mounted farther outboard of the 5 K manifolds, one of which is integral to the 100 K shield. The material of the 100 K thermal radiation shield is grade 1100 aluminum, chosen for its high thermal conductivity and light weight. The shield is fabricated from standard flat panels that are cut and formed to shape. The top portion of the shield is attached to the 100 K ring of the composite support post and is $\frac{1}{4}$" thick to support the

Figure 2.4.35: The tuner pre-bias operation for the ERL Injector.

weight of the cryogen manifolds and the lower portion of the shield, as shown in Fig. 2.4.36, at this stage of cold-mass assembly. A thermal model of the 100 K shield with an integral 100K manifold with heat loads from radiation, the composite post, and feedthroughs shows that the shield resides at less than 2 K above the manifold gas temperature [60].

Table 2.4.12: ERL main Linac cryomodule beamline components, their individual lengths, and the total length of the module.

	Component	Length (m)	Length (in)
	Gate valve	0.0750	2.953
	Taper	0.0500	1.9
Repeat 3 times	Large Cu beam tube	0.0794	3.125
	Large beam tube HOM absorber	0.0600	2.362
	Large Cu beam tube	0.0794	3.125
	Large Nb beam tube	0.1864	7.338
	Large beam tube transition	0.0307	1.211
	Cavity active #1	0.8059	31.729
	Small Nb beam tube	0.1495	5.885
	Small Cu beam tube	0.0794	3.125
	Small beam tube HOM absorber	0.0600	2.362
	Small Cu beam tube	0.0794	3.125
	Small Nb beam tube	0.1495	5.885
	Cavity active #2	0.8059	31.729
	Large beam tube transition	0.0307	1.211
	Large Nb beam tube	0.1864	7.338
	Large Cu beam tube	0.0794	3.125
	Large beam tube HOM absorber	0.0600	2.362
	Large Cu beam tube	0.0794	3.125
	Taper	0.0500	1.969
	BPM	0.0750	17.717
	Steering Coils	0.1500	5.906
	Quadrupole	0.4500	2.953
	Gate valve	0.0750	2.953
	Intermodule flex	0.3297	12.981
	Module Length	9.8213	386.667 (= 32.22 ft)
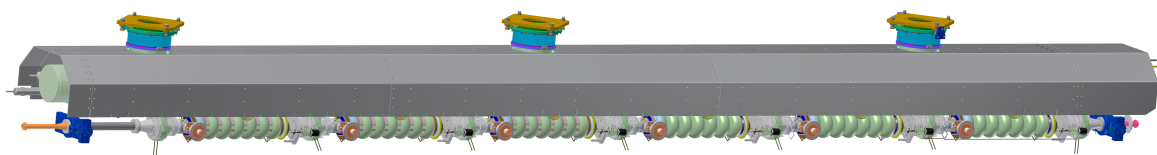
Figure 2.4.36: CAD model of the top portion of the 100K shield attached to the cold mass.

Figure 2.4.37: Photograph of the completed ERL Injector 100 K shield being wrapped with MLI.

After the cryogen manifolds and intercept jumpers are connected to the cold mass, low-thermal conductivity coax cable is routed from the cavity RF field probes, as well as the cabling from temperature sensors, helium level sticks, and other instrumentation. The lower half of the 100K shield is attached and the instrumentation cabling is thermally anchored to an instrumentation feed-through panel in the shield. The 100K shield is then wrapped with 30 layers of Multi Layer Insulation (MLI) and the cold mass is ready for insertion into the vacuum vessel. A photograph of the completed ERL injector 100K shield being wrapped with MLI is shown in Fig. 2.4.37.

Vacuum vessel and magnetic shield

The vacuum vessel must support the weight of the cold mass, withstand the atmospheric pressure differential, have ports for RF couplers and instrumentation, ports for gate valve actuators, mounts for support in the Linac tunnel, lifting points for transport, and end flanges to accommodate the bellows sleeve that link the cryomodules. The locations of the ports on the vacuum vessel are dictated by the cold-mass components. The vacuum vessel supports have some freedom of location, though vessel deformation under loading must not exceed acceptable limits. The maximum deformation of the top ports that bear the load of the cold mass by way of the composite posts was modeled and found to be 0.13 mm.

The majority of the material of the vacuum vessel will be carbon steel, with the vacuum

flanges that will have o-ring seals made of stainless steel to ensure that there will be no oxidation of the seal surfaces. The interior of the vacuum vessel will be burnished and painted with low vapor pressure vacuum compatible polyurethane paint. The exterior will likewise be burnished and painted with a marine paint.

Since carbon steel is a magnetic material, the vessel will be de-gaussed and care taken to not re-magnetize the vessel. Bench tests of carbon steel tubes show that local magnetization of the tube by permanent magnets can result in remnant magnetic fields in the interior of a few Gauss. The steel can be easily de-magnetized by intimate coils carrying 5300 Amp-turns, such that the remnant magnetic fields in the interior are reduced to about 250 mG. Further lining the interior of the vessel with Co-Netic mu-metal shielding then reduces the remnant magnetic fields in the interior to about 5 mG. However, the interior field could rise to the 25 mG level if the steel vessel is re-magnetized with permanent magnets. At the SRF cavity, these background magnetic fields are further attenuated by the cryogenic A4K magnetic shield [58] that will surround each SRF cavity. The cavity shield will reduce the magnetic field at the cavity to levels of $< 2\,\mathrm{mG}$, which then contributes negligible residual resistance to the SRF cavity surface.

The bellows section that mates adjacent cryomodule vacuum vessels will differ from the TTF-III bellows section since the ERL Linac will utilize at least one pneumatic gate valve per module. The pneumatic gate valves will allow any module to be isolated upon an interlock trip, and the pneumatic actuator will be connected through a port on the bellows section.

Cryomodule and cavity alignment

The prototype ERL injector cryomodule serves as the basis for the design of the cryomodule and cavity alignment system for the main Linac elements. Perhaps the most challenging element of the assembly procedure is the alignment of the quadrupole magnets to the needed tolerance (< 500 μm) lateral displacement with respect to the beam axis). Reference of the magnetic center of the quadrupoles to a reference point on the outside of the cryomodule when the magnet is cold will be essential for the successful operation of the ERL. The reproducibility of this translation will be one of the components of the study of the prototype Linac cryomodule. It will determine whether or not externally adjustable mounts for the quadruapoles will be required to be able to use beam based alignment techniques to align the quadrupoles to the required tolerance. The tolerances for the location of the accelerating cavities in the cryomodules are given in Tab. 2.1.6.

The assembly of the cryomodules will be carried out in clean rooms using fixtures and techniques very similar to the ones used for the assembly of the ERL injector cryomodule and the FLASH cryomodules and planned for the XFEL cryomodules. The finished ERL cryomodules will be transported in the tunnel in a manner similar to the transport of the LHC cryomodules with a tape or wire guided vehicle to their location and then translated onto their supports. A guided vehicle sized for the tunnel and beam line height can have a vertical lift capability of up to 25 cm with lateral push and pull sufficient to place and remove the cryomodules.

The interconnection and leak testing of the connected cryomodules will be carried out in a manner very similar to that used for the FLASH cryomodules and planned for the XFEL. Connection of the cryomodules to the cryogen supply lines and the warm transitions needed

Wall-plug Power for 64 Cryomodules, Q=2e10
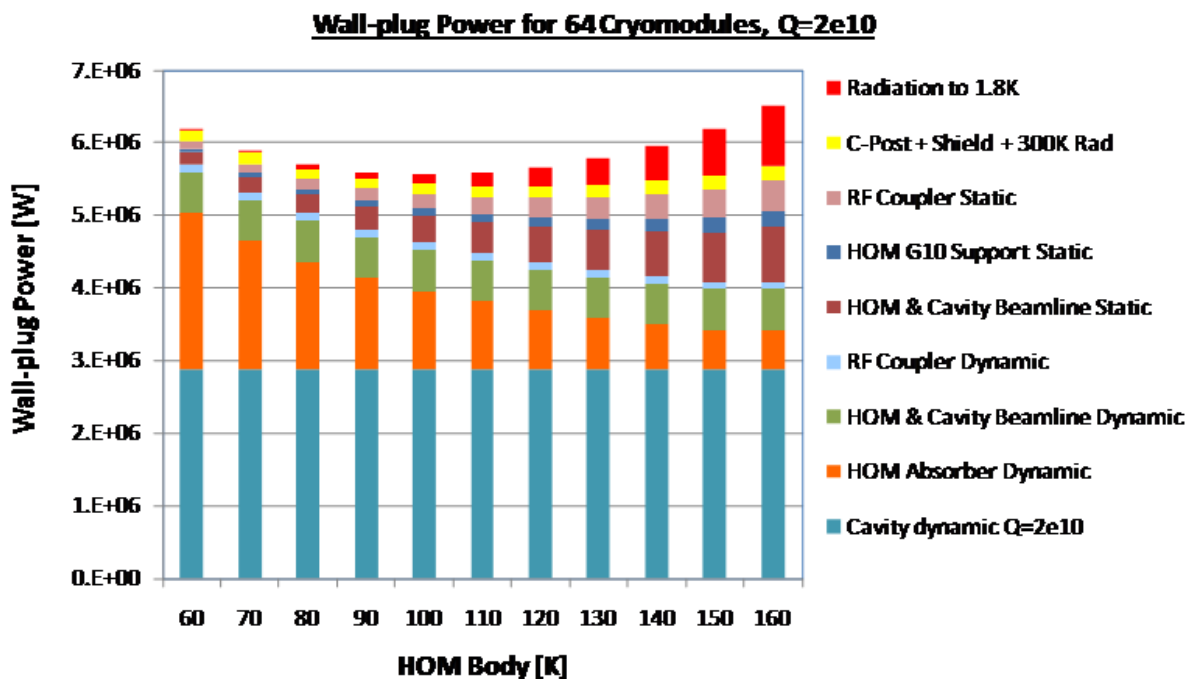
Figure 2.4.38: Wall-plug refrigeration power for a 64-module ERL main Linac with the SRF cavities having $Q_0 = 2 \times 10^{10}$ as a function of the intermediate intercept temperature.

to connect to other accelerator components will also be modeled after the ones planned for the XFEL.

Linac cryomodule heat loads

Having determined that the optimum cavity-operating temperature is 1.8 K, the optimal intermediate temperatures and corresponding heat loads are next to be determined. An important consideration arising from the configuration of the cavities is that the cavity beamtubes protruding from the cavity helium vessel must be superconducting. Considering the convenience of using helium gas just above boiling temperature, we choose 5 K as the next higher intermediate temperature. The thermal radiation shields and the HOM absorbers will need to be at some intermediate temperature between 5 K and 293 K. Detailed modeling shows a broad optimum at 100 K, as shown in Fig. 2.4.38. The models include analysis of the cold components and their material properties vs temperature as well as the Coefficients of Performance of refrigeration vs temperature derived from reports of manufacturers.

The distribution of wall-plug refrigeration power among cryomodule components for the 100 K intermediate temperature case is shown as a pie chart in Fig. 2.4.39. The SRF cavity dynamic load is about 52% of the total refrigeration load, with the dynamic HOM load being the next largest. The thermal gradient along the beamline due to the HOM loads being held at 100 K contributes the most to the static heat load. Table 2.4.13 lists the heat loads and wall-plug power per cryomodule and for the full Linac at the 100 K optimum.

263

Wall-plug Power for 64 Cryomodules, Q=2e10
Intermediate Temperature = 100K

Dynamic = 4.62 MW (83%)
Static = 0.94 MW (17%)
Total = 5.56 MW
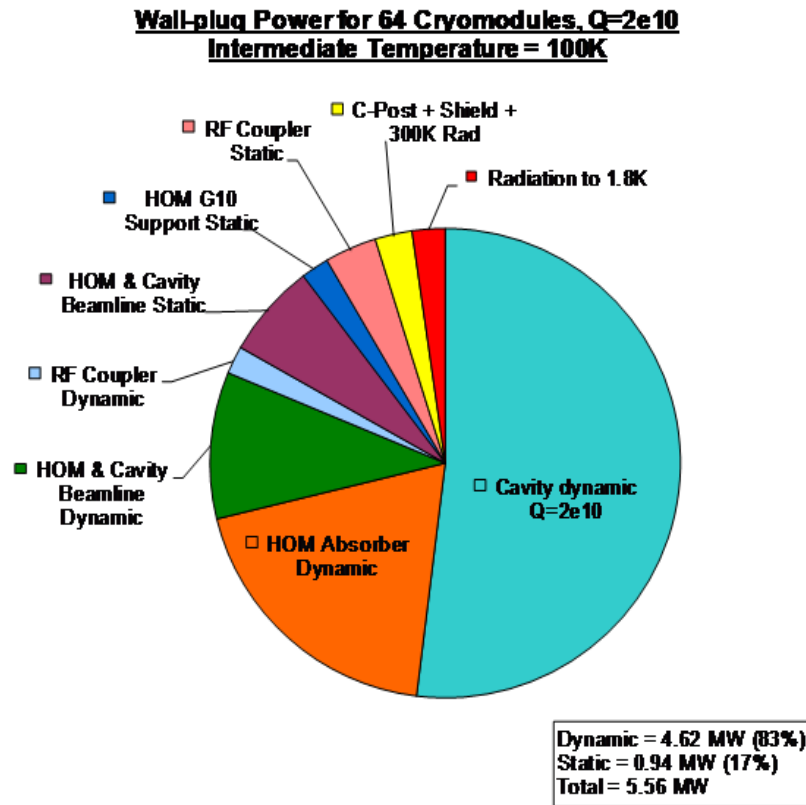
Figure 2.4.39: Distribution of wall-plug refrigeration power for the 64-module main Linac with a 100 K intermediate temperature.

As noted in the section on the cryogenic system and utilities, two helium refrigeration companies were asked to make studies of refrigerators that could handle the estimated thermal loads then estimated. In their studies, they utilized available suites of compressors and expanders with some practical compromises for control systems. The reports are available as references [61] [62]. The calculated operating electric powers using the available compressors and expanders are reported in the utilities section with a safety factor of 1.5 included.

To validate the predicted ERL heat loads listed in Tab. 2.4.13, Tab. 2.4.14 shows the predicted and typical measured static heat loads for the late-model FLASH TTF-III cryomodules [63]. The measured static load to 2 K is about 25% higher than predicted, but the other measured static loads are very close to the predicted values. These measured heat loads would be accommodated by a cryoplant that had a 50% capacity safety factor.

Cryomodule vacuum system

During operation the cryopumping of the accelerating cavities dominates all other pumping in the cryomodules. The challenge is to develop a pump down strategy that minimizes the risk of contamination of the accelerating cavities. A single piece of dust (even in μm size) will lead to field emission lowering Q_0 and a possibie quench of the cavity. A slow pump down sequence

Table 2.4.13: Heat loads and wall-plug power per cryomodule and for the full Linac with the SRF cavities having $Q_0 = 2 \times 10^{10}$.

Per Module	ERL Linac		
	Heat Load		Wall plug
1.8 Static (W)	7.28		5,240
1.8 Dynamic (W)	68.99		49,692
1.8 Total (W)	76.26		54,932
5 K Static (W)	45.16		8,882
5 K Dynamic (W)	25.65		5,045
5 K Total (W)	70.82		13,928
100 K Static (W)	50.09		598
100 K Dynamic (W)	1455.50		17,369
100 K Total (W)	1509.41		17,966
Module wall plug (W)			86,826
# modules		64	
Linac wall plug (W)			5.56×10^6
Safety factor		1.5	
Linac wall plug $\times$ safety factor (W)			8.34×10^6

Table 2.4.14: Predicted and typical measured static heat loads for late-model FLASH TTF-III cryomodules.

Per Module	FLASH Predicted	FLASH Measured
2K Static (W)	2.80	3.5
4.5K Static (W)	13.90	13
70K Static (W)	76.80	78

minimizes this risk. After the clean assembly of the cavity string in the cryomodule, the beam line will be pumped down and closed off by the beam line gate valves at either end of the cryomodule. The beam line will remain under vacuum during transport to the final location of the cryomodule. Cold cathode ion gauges will be used to monitor the beam line vacuum at all times. Leak testing will be carried out at each stage of the cryostat assembly following the procedures that were developed during the ICM assembly. These procedures were very similar to the one followed for the assembly of the FLASH cryomodules and the ones proposed for the XFEL cryomodules.

After placement of the cryo-modules in the Linac tunnel, interconnection vacuum beampipes will be installed to complete the Linac beamline vacuum. Each interconnection includes stainless steel beampipes, a flexible bellows (with proper RF-shielding or absorbers), a vacuum pumping port and gauge port. As the interconnections are enclosed in the Linac insulation vacuum walls, extensions are added to the pump/gauge port(s) to allow access to the port(s). Proper RF screens must be incorporated in the vacuum pump/gauge ports to minimize HOM heating at the screens. All components used on the interconnection (including ion pumps

and vacuum gauges) must be cleaned in a Class 100 clean room to remove particulates, and properly bagged for transportation to the site. A portable clean room capable achieving Class 100 will be set up to enclose the entire interconnection during the installation process.

The insulation vacuum will be maintained after initial pump down by the cryopumping of the outer surface of cavity helium vessels. There will be a pump port closed off by a suitable valve to allow this pump down. There will also be suitable ports to allow monitoring of the insulation vacuum along with appropriate gauges to continuously record the condition of the insulation vacuum. In case of sudden accidental release of cryogens inside the cryostat module, it will be equipped with safety blowoff ports that will require 10 psi overpressure to release.

Cryomodule instrumentation

Instrumentation for the cryomodule needs to be sufficient to correctly monitor the operation of the cryomodule. Since it will replicated 64 times for the full Linac, care needs to be take to avoid unnecessary monitoring. The required monitors would include helium level sensor for the JT/2-phase-pipe, temperature sensors in a number of locations with different types of sensors depending on the requirements, helium pressure sensors, and low level rf probes for accelerating gradient control. In addition there will be the tuner stepper and piezo drives, heaters and cavity alignment sensor if experience with the prototype cryomodule currently under construction indicates that this will be needed. As with other aspects of the main Linac cryomodules, the final design of the instrumentation package will be guided by the experience from the ICM, FLASH, and the planning for the XFEL.

2.4.9 Manufacturing plan

The Cornell ERL program is presently in the development phase to prove out the performance of key components of the facility. A great deal of insight has already been gained from the ERL injector and other prototypes at Cornell. A prototype main Linac cryomodule will be designed and fabricated in the next two years. Following this, a final cryomodule design will be completed that is compatible with all of the contiguous infrastructure of the ERL facility. The highlights of the development phase of the main Linac are described in the next section, followed by a description of the production phase.

Main Linac prototype cryomodule

As part of the Cornell ERL development program, prototypes will be fabricated and tested for the main Linac SRF cavity, RF coupler, HOM loads, and cavity tuner. After establishing satisfactory performance of the prototypes, production versions will be fabricated to complete one full Linac cryomodule. In parallel, the rest of the Linac cryomodule will be designed and a full prototype fabricated. There are several logistical options available that will allow the 10 m long prototype cryomodule to be assembled at Cornell with minimal modification to the existing facilities.

Testing of the prototype Linac cryomodule will include the following high-level tasks of increasing complexity:

- Cryogenic test of cooldown, cavity alignment, and heat leaks

- RF test of the cavity field, Q, and microphonics.

The first test of cooldown can easily be accomplished with existing Cornell facilities. The RF test would require a modest RF source and radiation shielding around the test area due to field emission from the cavities. A beam test of dressed, prototype cavities (i.e. cavities with HOM absorbers), coupler and field probes attached, will be beam tested at high beam current using the prototype injector to measure the cryogenic consequences of high current running on HOM absorber heating and search for trapped modes that could engender BBU in the full linac.

Main Linac 64-module production

The pace for production of the 64 cryomodules for the ERL main Linac is targeted to be 2 cryomodules per month, requiring about 2.7 years to complete the full Linac, with 1-2 more months added to produce spare cryomodules. The production pace is determined by the size of the test and assembly facility (for comparison refer to [64]). Since this facility is comprised of costly components, such as a clean room and refrigeration plant, and would likely have a one-time use, it is unlikely that an industrial partner would invest in such a facility without a longer term use. It is possible that such facilities that will be required by other laboratories for cryomodule production programs could be utilized if they have no commitments in the ERL production time frame.

An example layout of a cryomodule production facility is shown in Fig. 2.4.40, which is sized to produce 2 cryomodules per month. The facility includes:

- Clean room with HPR-cavity rinse, vacuum and gas feeds, equipment lock air showers, and 2 beamline string assembly areas

- High bay assembly area to accommodate 3 modules, overhead crane access, an adjacent overhead door to allow flatbed truck entry for loading and unloading

- Cryomodule test area with radiation shielding

- Cavity chemistry etch area

- Cavity $120°$ C vacuum bake area

- Cavity vacuum furnace for H_2 de-gassing ($800°$ C) or purification ($1400°$ C)

- Cavity tuning equipment

- Cavity vertical test pits with radiation shielding

- Cavity helium vessel Ti welding area

- De-ionized water production and storage

- Liquid helium refrigeration plant including an LN_2 tank for cavity vertical test and module tests
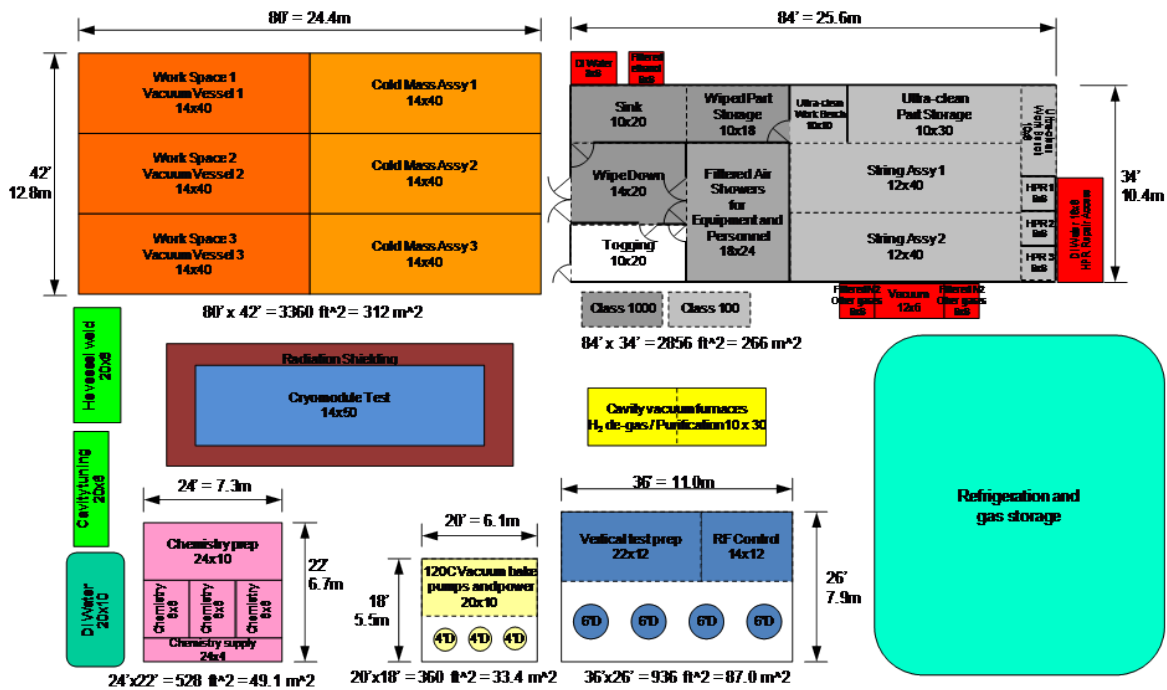
Figure 2.4.40: Block diagram of the space required for typical cryomodule production tasks to assemble two cryomodules per month.

The utilities for the production facility would include considerable AC power for the refrigeration plant and vacuum furnaces, a chilled water supply, and N_2 gas distribution from the LN_2 tank boil-off. It is possible that this facility could be erected in the existing Wilson Lab using existing portable shielding and the existing refrigeration plant.

2.4.10 Tunnel Filling

General Considerations

The tunnel is driven in two sections as shown in the overall layout Fig. 2.1.2. As discussed earlier, this affords the opportunity to compensate for wake-driven energy spread and other transit time manipulations. For both economy and proximity of the low-level RF electronics to the cavities being controlled, the electronics and high power amplifiers are placed as close to the cryomodules as shown in Fig. 2.4.41.

There is expected to be significant radiation in the Linac tunnels because of field emission in the cavities, and the magnitude of this can be estimated from experience at FLASH [65]. Accordingly the electronics racks will be shielded by 6-inch thick panels of heavy concrete as shown in Fig. 2.4.41. The intention is to have the panels on sliders so that they can be moved easily for access to the electronics behind.
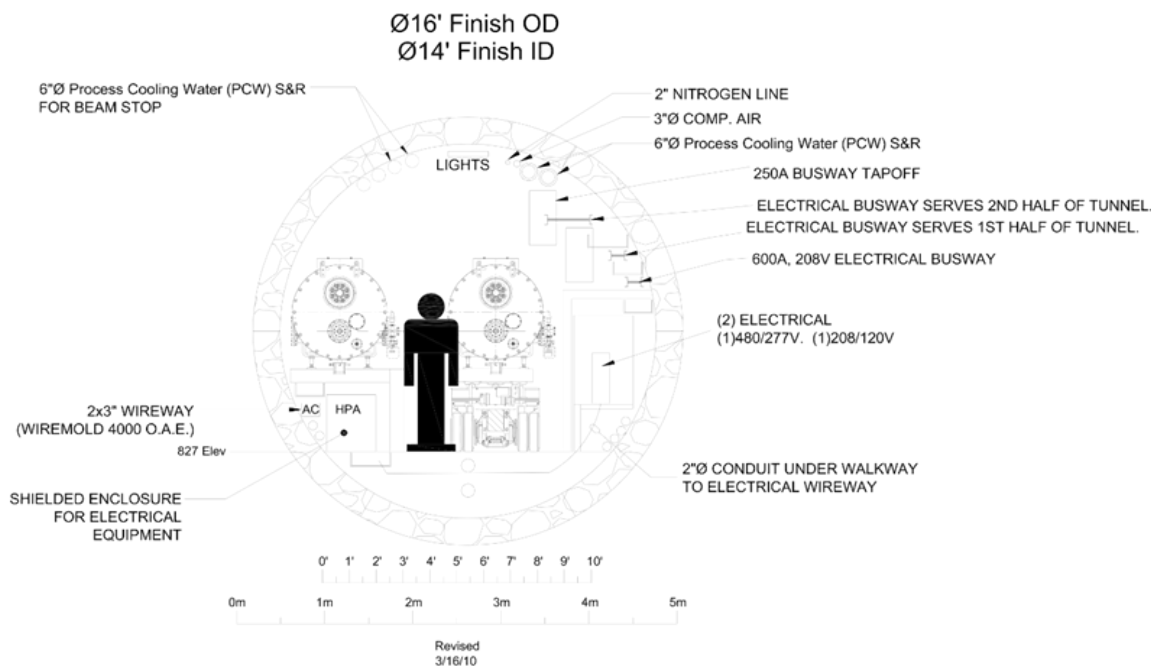
Figure 2.4.41: Tunnel cross-section showing safety provision for persons passing, equipment placement, shielding and utility pipes and ducts.

Utility considerations

Tunnel equipment requires water and forced air for cooling as well as electric power, clean nitrogen for venting, and compressed air for the activation of valves. The quantities are found in the utility tables in §4.4. A tentative disposition of the supply pipes and cables together with equipment placement is shown in Fig. 2.4.41.

Safety considerations

A primary determinant of the tunnel size is the requirement that a person can pass safely between the cryomodules in place and a cryomodule being transported in the tunnel for installation or removal as shown in Fig. 2.4.41. Ventilation by air at a velocity of 400 fpm is provided when the tunnel is occupied to sweep away helium spills, and fire barriers are provided to separate the tunnel from the x-ray halls. Proposals to achieve these safety objectives can be found in the architectural and conventional engineering report of the Arup company [66]. Helium safety matters are presented in §4.6.

References

[1] *The European X-Ray Free-Electron Laser Technical Design Report (XFEL), DESY 2006-097.* Technical report. ISBN 978-3-935702-17-1 http://www.xfel.eu/documents/technical_documents/.

[2] *International Linear Collider Reference Design Report, ILC-REPORT-2007-001.* Technical report.

[3] Petersen, B. *Some aspects of the layout and optimization for the cryogenic supply of superconducting linacs.* Nucl. Instr. and Meth. A, **557** (1), pages 280 – 286 (2006). ISSN 0168-9002. doi:DOI:10.1016/j.nima.2005.10.084. Energy Recovering Linacs 2005 - Proceedings of the 32nd Advanced ICFA Beam Dynamics Workshop on Energy Recovering Linacs.

[4] Rimmer, R. *Higher-order mode calculations, predictions and overview of damping schemes for energy recovering linacs.* Nucl. Instr. and Meth. A, **557** (1), pages 259 – 267 (2006). ISSN 0168-9002. doi:DOI:10.1016/j.nima.2005.10.080. Energy Recovering Linacs 2005 - Proceedings of the 32nd Advanced ICFA Beam Dynamics Workshop on Energy Recovering Linacs.

[5] Marhauser, F., *et al. HOM Survey of the First CEBAF Upgrade Style Cavity Pair.* In *The 23rd Particle Accelerator Conference*, pages 2123–2125. Vancouver, British Columbia, Canada (2009).

[6] Hammons, L. and H. Hahn. *HOM Absorber Development for BNL ERL Cryomodules.* In *The International Workshop on Energy Recovery Linacs, ERL09.* Ithaca, NY, USA (2009). http://accelconf.web.cern.ch/accelconf/ERL2009/html/author.htm.

[7] McIntosh, P. A., *et al. Assembly Preparations for the International ERL Cryomodule at Daresbury Laboratory.* In *14th International Conference on RF Superconductivity (SRF 2009)*, pages 864–868. Berlin, Germany (2009). http://accelconf.web.cern.ch/AccelConf/SRF2009/papers/thppo098.pdf.

[8] Liepe, M. and J. Knobloch. *Superconducting RF for energy-recovery linacs.* Nuclear Instruments and Methods in Physics Research Section A: Accelerators, Spectrometers, Detectors and Associated Equipment, **557** (1), pages 354 – 369 (2006). ISSN 0168-9002. doi:DOI:10.1016/j.nima.2005.10.099. Energy Recovering Linacs 2005 - Proceedings of the 32nd Advanced ICFA Beam Dynamics Workshop on Energy Recovering Linacs.

[9] Kugeler, O. *et al. Manipulating the intrinsic quality factor by thermal cycling and magnetic fields.* In *14th International Conference on RF Superconductivity (SRF 2009)*, pages 352–354. Berlin, Germany (2009). http://accelconf.web.cern.ch/AccelConf/SRF2009/papers/tuppo053.pdf.

[10] Valles, N., *et al. Testing of the Main-Linac Prototype CAvity in a Horizontal Test Cryomodule for the Cornell ERL.* In *Proccedings to 3rd International Particle Accelerator Concerence IPAC12* (2012). http://accelconf.web.cern.ch/accelconf/IPAC2012/papers/weppc075.pdf.

[11] Valles, N., *et al. Cornell ERL Main Linac 7-cell Cavity Performance in Horizontal Test Cryomodule Qualifications, WEPWO068.* In *Proccedings to 4rd International Particle Accelerator Concerence IPAC13* (2013).

[12] Kraemer, D., E. Jaeschke, and E. Eberhardt. *The BESSY Soft X-ray Free Electron Lasers.* Technical report, BESSY, Berlin (2004). ISBN 3-9809534-0-8.

[13] Mukherjee, B. *Measurement of Critical Radiation Levels at FLASH and their Relevance to XFEL.* FLASH seminar (May 29, 2007). http://flash.desy.de/sites/site_vuvfel/content/e870/e2179/infoboxContent2180/Flash-Seminar-290507.pdf.

[14] Liepe, M. and J. Knobloch. *Superconducting RF for energy-recovery linacs.* Nucl. Instr. and Meth. A, **557**, pages 354–369 (2005).

[15] Liepe, M. *et al. Status of the Cornell ERL Injector Cryomodule.* In *25th International Linear Accelerator Conference (LINAC10).* Tsukuba, Japan (2010). http://www.lns.cornell.edu/~liepe/webpage/docs/TU303.pdf.

[16] Myakishev, D. G. and V. P. Yakovlev. *The new possibilities of SuperLANS code for evaluation of axisymmetric cavities.* In *1995 Particle Accelerator Conference (PAC95)*, pages 2348–2350. Dallas, Texas, USA (1995). http://accelconf.web.cern.ch/AccelConf/p95/ARTICLES/MPC/MPC17.PDF.

[17] Valles, N. and M. Liepe. *Seven-Cell Cavity Optimization for Cornell's Energy Recovery Linac.* In *2009 International Workshop of RF Superconductivity (SRF2009)*, pages 538–542. Berlin, Germany (2009). http://accelconf.web.cern.ch/AccelConf/SRF2009/papers/thppo008.pdf.

[18] Hoffstaetter, G. and I. Bazarov. *Beam-Breakup Instability Theory for Energy Recovery Linacs.* Phys. Rev. ST-AB, **7**, page 054401 (2004). ISSN 0168-9002. doi:DOI:10.1103/PhysRevSTAB.7.054401.

[19] Myakishev, D. *CLANS2-A Code for Calculation of Multipole Modes in Axisymmetric Cavities with Absorber Ferites.* In *1999 Particle Accelerator Conference (PAC1999)*, pages 2775–2777. New York, NV, USA (1999). http://accelconf.web.cern.ch/AccelConf/p99/PAPERS/THA76.PDF.

[20] Buckley, B. and G. H. Hoffstaetter. *Transverse emittance dilution due to coupler kicks in linear accelerators.* Phys. Rev. ST Accel. Beams, **10** (11), page 111002 (Nov 2007). doi:10.1103/PhysRevSTAB.10.111002.

[21] Matsumoto, H., *et al. Experience with a Zero Impedance Vacuum Flange at He Super-Leak Temperature for the ILC.* In *The tenth European Particle Accelerator Conference, EPAC'06*, pages 753–755. Edinburgh, Scotland (2006).

[22] Zapfe-Duren, K., *et al. A New Flange Design for the Superconducting Cavities for TESLA.* In *The Eighth Workshop on RF Superconductivity*, pages 457–462. Abano Terme (Padova), Italy (1997).

[23] Kurokouchi, S., S. Morita, and M. Okabe. *Characteristics of a taper-seal type gasket for the Conflat ®; sealing system.* Journal of Vacuum Science Technology A: Vacuum, Surfaces, and Films, **19** (6), pages 2963 –2967 (November 2001). ISSN 0734-2101. doi: 10.1116/1.1415359.

[24] Conway, Z. and M. Liepe. *Electromagnetic and Mechanical Properties of the Cornell ERL Injector Cryomodule.* In *2009 Particle Accelerator Conference (PAC09)*, pages 915–917. Vancouver, Canada (2009). http://accelconf.web.cern.ch/AccelConf/PAC2009/papers/tu5pfp042.pdf.

[25] Padamsee, H. *RF Superconductivity for Accelerators.* John Wiley and Sons, Inc (1998).

[26] Amuneal Manufacturing Corp., Philadelphia, PA http://www.amuneal.com/.

[27] Singer, W. *et al. Preparation Phase for the 1.3 GHz Cavity Production of the European XFEL.* In *2010 International Particle Accelerator Conference (IPAC10)*, pages 3633–3635. Kyoto, Japan (2010). http://accelconf.web.cern.ch/AccelConf/IPAC10/papers/thoara02.pdf.

[28] Kneisel, P. *SRF cavity technology.* In *International Accelerator School for Linear Colliders 19-27 May 2006.* Sokendai, Hayama, Japan (2006). http://linearcollider.org/files/ilc_school/Lecture_11_Peter_Kneisel.ppt.

[29] Ciovati, G. *Effect of low-temperature baking on the radio-frequency properties of niobium superconducting cavities for particle accelerators.* Journal of Applied Physics, **96** (3), pages 1591 – 1600 (2004). ISSN 0021-8979. doi:DOI:10.1063/1.1767295.

[30] Weise, H. *Superconducting EF Structures - Test Facilities and Results.* In *2003 Particle Accelerator Conference (PAC03)*, pages 673–677. Portland, Oregon (2003). http://accelconf.web.cern.ch/Accelconf/p03/PAPERS/ROPC007.PDF.

[31] Valles, N. *et al. Exploring the Maximum Superheating Fields on Niobium.* In *14th International Conference on RF Superconductivity (SRF 2009)*, pages 406–410. Berlin, Germany (2009). http://accelconf.web.cern.ch/AccelConf/SRF2009/papers/tuppo072.pdf.

[32] Bosland, P. and B. Wu. *Mechanical study of the Saclay piezo tuner PTS (Piezo Tuning System).* Technical Report CARE-Note-2005-004-SRF, DAPNIA - CEA Saclay (2005). http://jra-srf.desy.de/sites/site_jra-srf/content/e86/e123/e125/e429/infoboxContent432/note-2005-004-SRF.pdf.

[33] Liepe, M., W.D.-Moeller, and S. Simrock. *Dynamic Lorentz Force Compensation with a Fast Piezoelectric Tuner.* In *The 2001 Particle Accelerator Conference (PAC 2001)*, pages 1704–1706. Chicago, Illinois, USA (2001).

[34] Bosotti, A., *et al. A fully automated device for checking XFEL piezo-tuner installation.* In *14th International Conference on RF Superconductivity (SRF 2009)*, pages 693–697. Berlin, Germany (2009). http://accelconf.web.cern.ch/AccelConf/srf2009/papers/thppo049.pdf.

[35] Pagani, C., *et al. ILC Coaxial Blade Tuner.* In *The tenth European Particle Accelerator Conference, EPAC'06*, pages 466–468. Edinburgh, Scotland (2006). http://accelconf.web.cern.ch/AccelConf/e06/PAPERS/MOPCH171.PDF.

[36] Neumann, A., *et al. Microphonics in CW TESLA Cavities and their Compensation with Fast Tuners.* In *12th International Conference on RF Superconductivity (SRF 2007)*, pages 377–383. Beijing, China (2007).

[37] Kugeler, O. *Cavity Tuners.* In *The International Workshop on Energy Recovery Linacs, ERL09.* Ithaca, NY, USA (2009). http://accelconf.web.cern.ch/accelconf/ERL2009/html/author.htm.

[38] Chojnacki, E. and W. J. Alton. *Beamline RF Load Development at Cornell.* In *1999 Particle Accelerator Conference*, pages 845–847. New York, USA (1999). http://accelconf.web.cern.ch/AccelConf/p99/PAPERS/MOP77.PDF.

[39] Tajima, T., *et al. HOM Absorbers of Superconducting Cavities for KEKB.* In *European Particle Accelerator Conference, EPAC'96*, pages 2127–2129. Barcelona, Spain (1996). http://accelconf.web.cern.ch/AccelConf/e96/PAPERS/WEPL/WEP061L.PDF.

[40] Shemelin, V., M. Liepe, and H. Padamsee. *Characterization of ferrites at low temperature and high frequency.* Nucl. Instr. and Meth. A, **557** (1), pages 268 – 271 (2006). ISSN 0168-9002. doi:DOI:10.1016/j.nima.2005.10.081. Energy Recovering Linacs 2005 - Proceedings of the 32nd Advanced ICFA Beam Dynamics Workshop on Energy Recovering Linacs.

[41] Chojnacki, E., *et al. DC Conductivity of RF Absorbing Materials.* In *14th International Conference on RF Superconductivity (SRF 2009)*, pages 643 –647. Berlin, Germany (2009). http://accelconf.web.cern.ch/AccelConf/srf2009/papers/thppo035.pdf.

[42] Sekutowicz, J. *Higher Order Mode Coupler for TESLA.* In *The Sixth Workshop on RF Superconductivity*, pages 426–439. Virginia, USA (1993). http://accelconf.web.cern.ch/AccelConf/SRF93/papers/srf93g04.pdf.

[43] Watanabe, K., *et al. New HOM coupler design for ILC superconducting cavity.* Nucl. Instr. and Meth. A, **595** (2), pages 299 – 311 (2008). ISSN 0168-9002. doi:DOI:10.1016/j.nima.2008.06.048.

[44] Kneisel, P. *et al. Testing of HOM Coupler Designs on a Single Cell Niobium Cavity.* In *2005 Particle Accelerator Conference*, pages 4012–4014. Knoxville, Tennessee (2005). http://epaper.kek.jp/p05/PAPERS/TPPT077.PDF.

[45] Kim, S. *et al. Study on Fault Sccenarios of Coaxial Type HOM Couplers in SRF Cavities.* In *2006 Linear Accelerator Conference (LINAC06)*, pages 770–772. Knoxville, Tennessee (2006). http://accelconf.web.cern.ch/accelconf/l06/PAPERS/THP081.PDF.

[46] Kazimi, R., *et al. Observation and Mitigation of Multipass BBU in CEBAF.* In *The eleventh European Particle Accelerator Conference, EPAC'08*, pages 2722–2724. Genoa, Italy (2008). http://accelconf.web.cern.ch/AccelConf/e08/papers/wepp087.pdf.

[47] Campisi, I. *et al. CEBAF Cryomodules: Test Results and Status.* IEEE Transactions on Magnetics, **27** (2), pages 2300–2303 (1991). ISSN 0018-9464. doi:DOI:10.1109/20.133677.

[48] Huang, Q., *et al. Carbon Nanotube RF Absorbing Materials.* In *14th International Conference on RF Superconductivity (SRF 2009)*, pages 648–651. Berlin, Germany (2009). http://accelconf.web.cern.ch/AccelConf/srf2009/papers/thppo036.pdf.

[49] Belomestnykh, S. *Overview of input power coupler developments, pulsed and CW.* In *The 13th Workshop on RF Superconductivity*, pages 419–423. Beijing, China (2007).

[50] Belomestnykh, S., *et al. High average power fundamental input couplers for the Cornell University ERL: requirements, design challenges and first ideas.* Technical Report Cornell LEPP Report ERL 02-8 (2002).

[51] Moeller, W.-D. *High power coupler for the TESLA Test Facility.* In *9th Workshop on RF Superconductivity*, pages 577–581. Santa Fe, NM,USA (1999). For the TESLA Collaboration.

[52] Dwersteg, B., *et al. TESLA RF Power Couplers Development at DESY.* In *Proceedings of the 10th Workshop on RF Superconductivity*, pages 443–447. Tsukuba, Japan (2001).

[53] Veshcherevich, V., *et al. High power tests of input couplers for Cornell ERL injector.* In *The 13th Workshop on RF Superconductivity*, pages 517–519. Beijing, China (2007).

[54] Veshcherevich, V. and S. Belomestnykh. *Input coupler for main linac of Cornell ERL.* In *The 14th International Conference on RF Superconductivity*, pages 534–545. Berlin, Germany (2009).

[55] Yla-Oijala, P. *Electron multipacting in TESLA Cavities and Input Couplers.* Particle Accelerators, **63**, pages 105–137 (1999). http://cdsweb.cern.ch/record/1120324/files/p105.pdf.

[56] A. Mikhailichenko and T. Moore. *Simple Procedure for Superconducting Coil Winding.* In *The 2001 Particle Accelerator Conference (PAC 2001)*, pages 3645–3647. Chicago, IL (2001).

[57] Lorenz, R. *et al. Measurement of the Beam Position in the TESLA Test Facility.* In *1996 Linear Accelerator Conference (LINAC96)*, pages 527–529. Geneva, Switzerland (1996). http://accelconf.web.cern.ch/accelconf/l96/PAPERS/TUP76.PDF.

[58] Amuneal Manufacturing Corp. Technical report, Philadelphia, PA, USA, Amumetal 4k (A4K) (2010). http://www.amuneal.com/magnetic-shielding/idea-share/whats-new-cryogenic-shielding.

[59] Chojnacki, E., *et al. Design and Fabrication of the Cornell ERL Injector Cryomodule.* In *The eleventh European Particle Accelerator Conference, EPAC'08*, pages 844–846. Genoa, Italy (2008). http://accelconf.web.cern.ch/AccelConf/e08/papers/mopp123.pdf.

[60] Chojnacki, E., *et al.* *Cryogenic Heat Load of the Cornell ERL Main Linac Cryomodule.* In *The 14th International Conference on RF Superconductivity*, pages 638–642. Berlin, Germany (2009). http://accelconf.web.cern.ch/AccelConf/SRF2009/papers/thppo034.pdf.

[61] *Cryogenic Plant Study and Budgetary Estimate for ERL Facility, Proposal, November 2006.* Proposal submitted to CLASSE by Linde Kryotechnik, AG. Report is on file at Cornell.

[62] *Helium Refrigeration system for the ERL Cornell Project – Technical Proposal, December,.* Technical report, Air Liquid (2006). Proposal submitted to CLASSE, Modified May, 2010.

[63] Peterson, T. *An Overview of the International Linear Collider (ILC) Cryogenic System.* Cryogenic Operations Workshop at SLAC (May 09, 2006). http://www.slac.stanford.edu/econf/C0605091/present/PETERSON.PDF.

[64] Napoly, O. *XFel Module Assembly at CEA-Saclay.* Fermilab Accelerator Seminar (February 17, 2009). http://beamdocs.fnal.gov/AD-public/DocDB/ShowDocument?docid=3311.

[65] R.J. Hernandez Pinto, M. V., M. Otto. *Radiation Measurements in the FLASH Tunnel in Summer 2006.* Technical report, DESY, Hamburg (2006). DESY Technical Note 2006-04.

[66] ARUP. *Energy Recovery Project Definition Design, Volume I Report.* Technical report (2010).